CHAPTER 1

Concept of Structure–Property Relationships in Molecular Solids and Polymers

1.1 Introduction

Low molar mass organic molecules and polymeric materials are often found as solids and their physical properties are a consequence of the way in which the molecules are organized: their *morphology*. The morphology is a result of specific molecular interactions which control the processes involved in the individual molecules packing together to form a solid phase. Depending on the extent of the molecular organization, a crystalline solid, liquid crystals or amorphous solid may be formed. As we shall see later, the organization that is created at a molecular level sometimes also tells us about the macroscopic form of the material, but in other cases it does not, hence the subtitle of the book: 'from nano to macro organization'.

Synthetic polymers, often referred to as *plastics*, are familiar in the home as furniture, the frames for double glazed windows, shopping bags, furnishings (carpets, curtains and covering for chairs), cabinets for televisions and paper and paint on the walls. Outside the house plastics are used for rainwater pipes, septic, water and fuel storage tanks, garden furniture, water hoses, traffic cones and sundry other items which we see around us. Removal of all articles containing polymers from a room would leave it bare. Synthetic plastics form the basis for many forms of food packaging, containers for cosmetics, soft drink containers and the trays used in microwave cooking of food. Natural polymers such as wood, cotton and wool all exhibit a high degree of order and many biopolymers play a critical role in the human body.

Whilst a focus of this monograph is structure in polymeric materials, many of the factors that control the organization of these big molecules are best studied with lower molecular weight analogues. It is therefore appropriate to spend some time understanding small molecular systems before the consideration of the complexity of polymers is undertaken.

The physical properties of a material are dictated by its ability to self-assemble into a crystalline form. Polymer chemists have for many years sought to establish structure–property relationships that predict various physical properties from of knowledge the chemical structure of the polymer. Staudinger[1,2] recognized that polymers or macromolecules are constructed by the covalent linking of simple molecular repeat units. This structure is implied in the phrase *poly* meaning many and *mer* designating the nature of the repeat unit.[3,4] Thus poly(ethylene) is the linkage of many ethylene units:

$$H_2C{=}C_2H \rightarrow -(CH_2{-}CH_2)_n-$$

Recognition of the nature of this process of *polymerization* made it possible to produce materials with interesting and useful properties, and brought about the discipline of polymer science. The value of 'n' indicates the number of monomers in the polymer chain.

In the last forty years, a very significant effort has been directed towards understanding the relation between the chemical structure of the polymer repeat unit and its physical properties.[5,6] In the ideal situation, knowing the nature of the repeat unit it should be possible to be able to determine all the physical properties of the bulk solid. Whilst such correlations exist, they also require an understanding of the way in which the chemical structure will influence the chain–chain packing in forming the solid. Similar correlations can be created for the understanding of other forms of order in lower molecular weight materials.

1.2 Construction of a Physical Basis for Structure–Property Relationships

Why do structure–property relations apparently work?

1.2.1 Ionic Solids

In order to understand the basis for structure–property correlations, it is appropriate to consider the structure of simple ionic solids. A solid sodium chloride single crystal (Figure 1.1) can be constructed starting from the atomic species of sodium [Na^+] and chlorine [Cl^-].[7] Since each ion carries a single charge, pairing the ions to form an NaCl *pair* would create a lower energy state. This *pair* will have a minimum separation and would be charge neutral. The line formed between the two atoms can be considered to lie on the x-axis. If another *pair* of atoms is brought close to the first pair, then once more a minimum energy situation would be created if the two pairs of atoms are aligned but their orientations are in the opposite sense. This arrangement will have a lower energy than the isolated pair and the distance between the atoms will be slightly reduced compared with the isolated pair. A further reduction in energy will accompany bringing to the cluster a further pair of atoms. This latter pair will

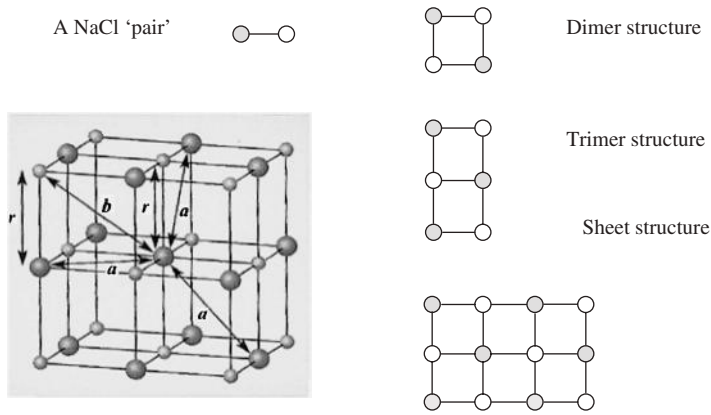

Figure 1.1 NaCl-type of crystal structure.

align in an opposite sense to the pair to which it attaches itself. Once more there will be a small change of separations to reflect the formation of a lower energy state. It is relatively easy to see that this process can be repeated and a sheet of atoms would be formed. As we will see later this same principle is used in considering attachment and growth of molecular and polymeric crystals.

The sheet of atoms formed by the process described above is not the lowest energy structure that can be formed. If this original sheet is sandwiched between similar states such that each of the Na and Cl atoms becomes surrounded by atoms of the opposite sign then a true minimum will be observed. If this order structure cannot be formed, because the entropy (disorder) is high, then the ensemble of atoms will be in the melt or gaseous state.

In the case of the NaCl crystal, this lowest energy structure is a cubic close-packed structure and results from each atom having six neighbouring atoms of opposite sign. Changes in the size of the ions and their charges lead to different types of packing being favoured. However, it is relatively easy to see that an *average energy* can be ascribed to a basic unit of the structure and this will reflect the physical properties of the bulk. Whilst the energy of the first pair can be calculated explicitly, adding additional elements means that the force field has to be averaged and will give rise to the problem of how one calculates the interaction of many bodies all interacting. The energy is the result of electrostatic (Coulombic) interactions between unit charges and in principle can be calculated by averaging all the interactions that will act on an atom chosen as the reference. The above example illustrates not only the lowering of the energy by surrounding an atom by other atoms but it illustrates that atoms in the surface will have a higher energy and we will meet this concept again when we consider polymers organizing at interfaces.

The total number and relative magnitudes of the Coulombic interactions and whether they are attractive or repulsive are taken into account by using a factor

known as the *Madelung* constant, A. The lowest energy for the lattice $\Delta U(0\text{K})$ (Coulombic) can for an ionic lattice be expressed by

$$\Delta U(0\text{K})\ (\text{Coulombic}) = \left(\frac{LA|z_+||z_-|e^2}{4\pi\varepsilon_0 r}\right) \tag{1.1}$$

where $|z_+|$ and $|z_-|$ are, respectively, the modulus of the positive and negative charges, e is the charge on the electron ($=1.602 \times 10^{-19}$ C), ε_0 is the permittivity of a vacuum ($=8.854 \times 10^{-12}$ F m^{-1}), r is the intermolecular distance between the ions (in m), L is Avogadro's number (6.022×10^{-23} mol^{-1}) and A is the Madelung constant.

The Madelung constant takes into account the different Coulombic forces, both attractive and repulsive, that act on a particular ion in a lattice. In the NaCl lattice, six Cl^- atoms surround each Na^+ atom. The coordination number -6 describes the number of atoms which surround the selected reference atom. X-ray analysis indicates that each atom is a distance of 281 pm from its nearest neighbour. To calculate the Madelung constant we consider the four unit cells that surround the selected reference atom. Firstly there are twelve Cl^- ions each at a distance a from the central ion, and the Cl^- ions repel one another. The distance a is related to r by the equation

$$a^2 = r^2 + r^2 = 2r^2 \text{ and thus } a = r\sqrt{2} \tag{1.2}$$

Next there are eight Na^+ ions each at a distance b from the central Cl^- ion, giving rise to attractive forces. Distance b is related to r by the equation

$$b^2 = r^2 + a^2; \quad b^2 = r^2 + (r\sqrt{2})^2; \quad b^2 = 3r^2; \quad b = r\sqrt{3} \tag{1.3}$$

Further attractive and repulsive interactions occur, but as the distance involved increases, the Coulombic interactions decrease.

The Madelung constant, A, contains terms for all the attractive and repulsive interactions experienced by a given ion, and so for the NaCl lattice the Madelung constant is given by

$$A = 6 - \left(12 \times \frac{1}{\sqrt{2}}\right) + \left(8 \times \frac{1}{\sqrt{3}}\right) - \ldots \tag{1.4}$$

where the series will continue with additional terms for interactions at greater distances. In general, the larger the distances involved the smaller the contribution to the energy and the magnitude of A is dominated by the first and second neighbour interactions. Note that r is not included in the equation and the value of A calculated is for all sodium chloride types of lattices. Thus the Madelung constant is a single parameter that describes with other constants the energy of the lattice. In this system, the dominant forces are electrostatic and hence the picture of the atoms as spheres is a reasonable approximation to reality. The physical properties of sodium chloride can be calculated on the basis of a knowledge of the interaction between the atoms. This simple principle

can be extended to molecular species and to polymers. Obviously as the molecular structure becomes more complex the problem of the calculation increases dramatically; however, the additivity principle often applies and reflects the appropriateness of *mean field approximations* in many cases. The *A* parameter is associated with a specific atom pair and changing the atoms will give another characteristic value. Examination of a number of pairs of such systems allows specific interactions to be identified which can be used additively to predict the properties of an unknown system. In the case of an atomic solid the dominant forces are electrostatic. In most organic materials, short-range van der Waals repulsive and attractive interactions are dominant and longer range electrostatic and dipolar interactions play a very important role in defining the final structure.

1.2.2 The Crystal Surface

A further important feature of physical predictions can be obtained from this simple model. If we consider the surface of the solid, it is relatively easy to see that the atoms in this sheet will have a slightly different energy from those in the bulk of the material. This excess energy was recognized by Gibbs and discussed in terms of *surface tension* for a liquid. Bringing a further layer of atoms to this surface—crystal growth—can lower the energy of the atoms in the surface or if the atoms are different this process is usually considered as absorption. NaCl is a very simple model and the question we will next address is whether this concept can be applied to covalently bonded systems.

1.2.3 Molecular Solid

The next step in the development of an understanding of the physical properties of polymers is to consider how a molecule such as dodecane forms single crystals. Crystals of dodecane are usually grown from a solution or from the melt by slow cooling. The dodecane molecule, CH_3–$(CH_2)_{10}$–CH_3 (Figure 1.2), has an all-*trans* conformation as a consequence of nonbonding repulsive interactions between hydrogen atoms on neighbouring carbon atoms. A higher energy *gauche* state exists in which the interaction between neighbouring atoms is greater than in the *trans* conformation. The distribution between the *gauche* and *trans* conformations is predictable in terms of statistical mechanics.

Following the process used to create the NaCl crystal, a low-energy state can be achieved if two of these all-*trans* dodecane molecules are brought close together and aligned. Following the logic presented above, a lowering of the energy will occur and a further reduction will be observed when a third and fourth molecule are brought up to the first two. This process would produce a layer of molecules extending in the y–z plane. A further reduction in energy would be achieved by the addition of another sheet of molecules on top of the first and so forth. The forces that govern the interaction between the molecules

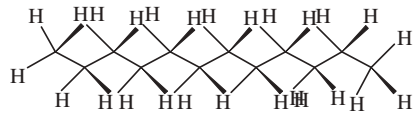

trans conformation of dodecane

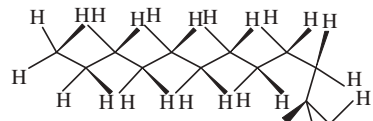

gauche conformation for dodecane

Figure 1.2 *Trans* and *gauche* conformations in dodecane.

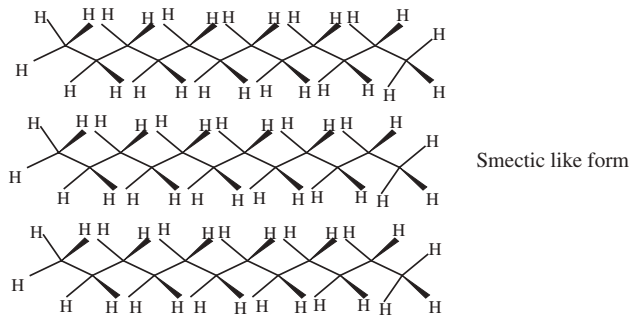

Smectic like form

nematic like form

Figure 1.3 *Smectic* and *nematic* forms of packing in dodecane.

are now van der Waals interactions rather than the stronger electrostatic Coulombic interactions.

A question that could be asked is whether an even lower energy would arise if the molecules were to pack in a staggered array rather than being perfectly aligned. The proposed difference in order gives rise to *nematic* and *smectic*

phases in liquid crystalline phases (Figure 1.3). The staggered form is analogous to the *nematic* phase, with the molecules aligned in one direction but disordered in at least one other direction. In the *smectic* phase, the molecules are aligned in a plane but may be misaligned between the layers and are closer to the lowest energy crystalline ordered structure than the *nematic* phase. The *nematic* will have a number of methyl–ethylene bond interactions and these will be less favourable than the ethylene–ethylene bond interactions. The topic of liquid crystals is discussed more fully in Chapter 3.

Dodecane can exist in a number of higher energy forms in which one or more *gauche* structures are incorporated into the chain backbone. The process of conformational change will involve the hydrogen atoms on neighbouring carbon atoms being brought into an eclipsed conformation. This eclipsed conformation is a higher energy state and inhibits the free exchange between the *trans* and the *gauche* conformation in which the energy has once more been minimized.

At any temperature above absolute zero there will be a finite population of the higher energy *gauche* state dictated by the Boltzmann distribution:[8]

$$\frac{n_g}{n_t} = \frac{g_1}{g_2} \exp\left(\frac{-\Delta E}{RT}\right) \tag{1.5}$$

where ΔE is the energy difference between the *gauche* and *trans* states, g_1 and g_2 are, respectively, the degeneracy of the *trans* and *gauche* states at the temperature T and R is the gas constant. Since there are two gauche states, which are energetically degenerate, then the statistical factor is $\frac{1}{2}$ and ΔE is the energy difference between the *trans* and *gauche* states. This temperature dependence of the conformation of many molecular species plays a critical role in determining their behaviour when cooled to form a solid. At the temperature of the melt phase, there will be expected to be a significant population of *gauche* conformations. The *trans* conformation is the lowest energy state and is able to nucleate crystal growth.

The molecules which are in the surface will also have the lowest energy state and whilst there will be defects in the crystal there is no reason to believe that the surface structure should not be different from that of the bulk. The energy of interaction between the dodecane chains can be seen to be the average of the interaction of one methylene chain with another. As with the case of NaCl, a single interaction parameter should describe the physical properties of the solid. In creating this average energy the interactions of the end chains needs to be included. Studies of the melting points for the paraffin homologous series indicate that the lower members lie on different curves depending whether they have odd or even numbers of carbon atoms.[9–11] The equilibrium crystal structure is also different and can in part be explained by the way in which the methyl groups at the end of the molecules interact. As the chains become longer this odd–even effect disappears and is nonexistent for n greater than about 20 (Figure 1.4).

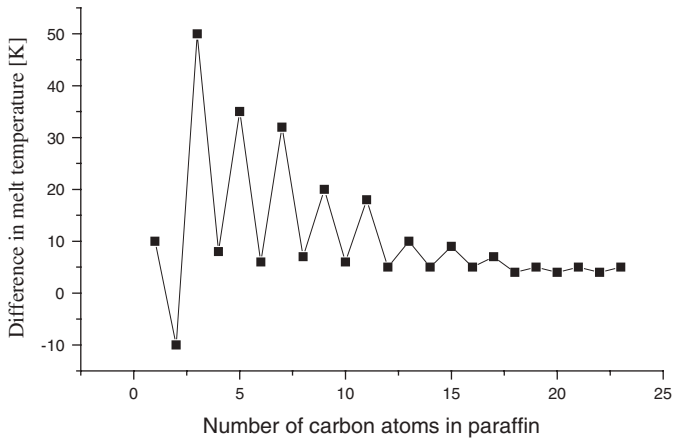

Figure 1.4 Difference between freezing points of successive paraffins.

1.2.4 Low Molar Mass Hydrocarbons

The dodecane molecule in the liquid state will be expected to have on average one *gauche* state per molecule at room temperature[12] but in the solid, however, it will have a structure that is predominantly made up of the all-*trans* form. The enthalpy of interaction compensates for the required loss of entropy in the crystallisation process. In the case of the *n*-alkanes, the bond lengths for the C–C and C–H bonds are, respectively, 1.5 and 1.10 Å and the C–C–C bond angle is 112° from studies of the solid.[13,14] The H–C–H bond angle has been found to be 109°. The conformational changes can be described by a potential energy diagram (Figure 1.5).

Abe *et al.*[15] have shown that the potential energy profile can be reproduced by selecting a barrier to the interchange between the *trans* and *gauche* forms of 12 540 J mol^{-1} and the energy difference between the two conformations has a value of 2090 J mol^{-1}. The energy and barrier to rotation are a result of nonbonding repulsive and attractive interactions between the hydrogen–hydrogen and hydrogen–carbon atoms on neighbouring carbon atoms.

The original calculations carried out by Scott *et al.*[16] used simple pairwise interactions. More sophisticated quantum mechanical calculations have confirmed the correctness of these original predictions. The conformation of *n*-butane, the simplest *n*-alkane, is described by three rotation angles (Figure 1.6).

Conformation energies computed for this molecule[15] in the neighbourhood of the *trans* and *gauche* minima for bond 2 indicate that the *gauche* minimum occurs at 112.5° rather than the expected 120° and has a value of 2215 J mol^{-1}.

Similar calculations for the next member of the series, *n*-pentane, give a potential surface, the contours being drawn in values of 1 kcal mol^{-1} (4.18 kJ mol^{-1}) above the minimum conformation, the *trans–trans* [tt] conformation

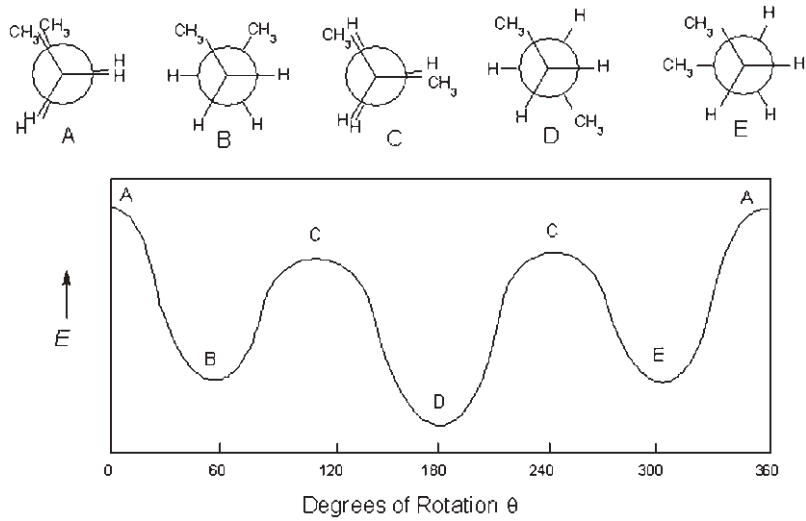

Figure 1.5 Potential energy curve obtained for *n*-butane for rotation about the 2,3 central bond of the molecule.

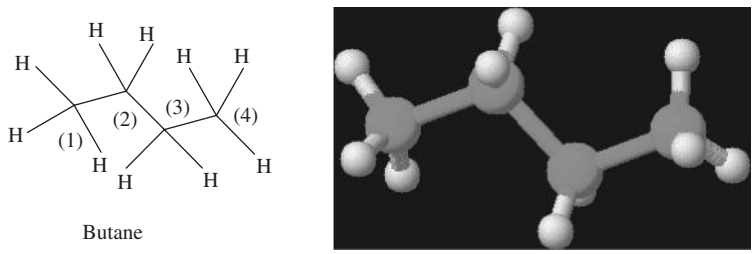

Figure 1.6 Labelled structure for *n*-butane. The angle ϕ_1 is the torsional angle for the bond joining C1 and C2, ϕ_2 is the torsional angle for the bond joining C2 and C3, ϕ_3 is the torsional angle for the bond joining C3 and C4.

with $\phi_2 = \phi_3 = 0$ (Figure 1.7). For the purpose of this calculation, the terminal methyl groups were fixed at $\phi_1 = \phi_4 = 0$, *i.e.* the terminal methyl groups are fixed in their staggered conformations. The portion of the energy surface for $\phi_2 < 0$ is produced by inversion through the origin in the ϕ_2, ϕ_3 plane.

The $tg^{\pm}$ and $g^{\pm}t$ minima are equivalent to those for *n*-butane. The g^+g^+ and g^-g^- minima (not shown) occur in the vicinity of $\phi_2 = \phi_3 = \pm 110^\circ$. Thus the *gauche* minima for two adjoining bonds in *gauche* conformations of the same sign are mutually displaced a few degrees from the values ($\sim 112.5^\circ$) which would be assumed by each if both of its neighbours were *trans*.

The *trans* minima for neighbouring bonds 1 and 4 are also perturbed a few degrees. These effects arising from subtle interactions between pairs of H atoms on third neighbour carbons are small. The calculated energy for the g^+g^+ pair is 4932 kJ mol^{-1}, which is close to twice the value for one *gauche* bond alone.

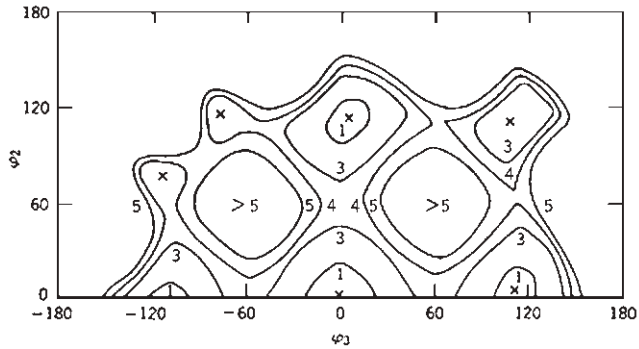

Figure 1.7 Energy contour map for the internal rotation in *n*-pentane with $\phi_1 = \phi_4 = 0$. The contours are shown at intervals of 1 kcal mol^{-1}. Minima are indicated by $\times$.

Hence the energy for neighbouring bonds in *gauche* states of the same sign may be treated as being additive. It is also interesting to note that the breadth of the *gauche* well is little affected by its neighbour.

Surprisingly, calculations of methylheptane[17] and methylpentane[18] have shown that the predictions are very close to the experimental values. These molecules, despite the fact that they can exhibit complex potential surfaces, are exhibiting simple additive interactions in the same way as that observed in *n*-butane. Once more this establishes the possibility of using a molecular description to be able to predict the physical properties of these molecules.

1.2.5 Poly(methylene) Chains

In principle, the poly(methylene) chain would represent a more complex potential surface than that of pentane. The number of different conformations following this simple scheme is 3^{n-3}. A typical polymer molecule may have 10000 carbons and thus $3^{9997} \approx 10^{4770}$ conformations, *i.e.* an enormously large number of states. Surprisingly the energy surface obtained is essentially identical to that of *n*-pentane (Figure 1.7). The energy surface obtained suggests a five-fold scheme, with rotational states at angles $\phi_i \approx 0$, 77, 115, -115, -77°. These could be labelled t, g^{*+}, g^+, g^-, g^{*-}, with combinations $g^{\pm}g^{\pm}$ forbidden by their large energies. A further simplification that is found to be practically justified is the deletion of the g^{*+} and g^{*-} states since they are assumed to have energies which are close to the $g^{*\pm}g^{\pm}$ and $g^{\pm}g^{*\pm}$ states. The result of this approximation is that the five-fold scheme is replaced by a three-fold representation that resembles that shown in Figure 1.5. However, the smaller numbers of minima have properties that represent the effects of a larger number of nonbonding interactions. The values of the energies that are usually

used to describe the curve are 2.1 kJ mol^{-1} for the energy difference and 8.4 kJ mol^{-1} for the eclipsed state. Flory and others have shown that this simple approach can be applied successfully to many other chains.[19,20] The basis of the so-called Rotational Isomeric States Model (RISM) used extensively for the prediction of the physical properties of polymers is thus based on simple additive effects of nonbonding interactions between the atoms attached to the backbone carbon atoms.[20–22]

1.3 Conformational States of Real Polymer Molecules in the Solid State

In a real polymer system, the chain will attempt to crystallize in the lowest energy state. The lowest energy state for a polymer such as poly(methylene) will be an extended all-*trans* structure. Studies of single crystals of poly(methylene) formed from dilute solution resemble the predicted structure of a single crystal; however, there are a number of other factors which will influence the nature of the crystal structure or morphology observed. It is appropriate to divide polymers into various types depending on their chemical repeat unit.

1.3.1 Crystalline Polymers

Polymers such as poly(methylene) which have a high degree of symmetry associated with the polymer backbone have a simple potential energy surface. There will exist a finite possibility of finding chains having long sequences of *trans* elements that are favourable for the formation of nucleating sites for crystal growth. The *gauche* elements are less readily packed and hence will be accommodated at the limits of these aligned *trans* orientated regions. If the crystals are grown at low temperature the *gauche* content will be predicted to be low and hence the 'defects' can be accommodated at the interfaces. However, as we shall see later, the real situation is rather different and more detailed considerations of the way in which the chains can pack as well as the structure of the backbone are required to be able to interpret the structure of the solid state for a particular polymer. In general, however, if the polymer has a simple backbone structure it is likely to form a crystalline polymer solid. Thus polytetrafluoroethylene, like polyethylene, forms a crystalline phase. Other polymers with simple structures are poly(ethylene oxide), poly(methylene oxide), poly(propylene oxide), poly(isotactic propylene), *etc*. Interestingly the isotactic polypropylene polymer forms a hard rigid crystalline solid, whereas the syndiotactic or atactic polymers are soft disordered materials with low levels of crystallinity. The tactic forms of polypropylene are shown in Figure 1.8.

In the case of isotactic polypropylene, the methyl groups dictate a helical conformation to the backbone and this results in a regular structure which is able to crystallize readily.

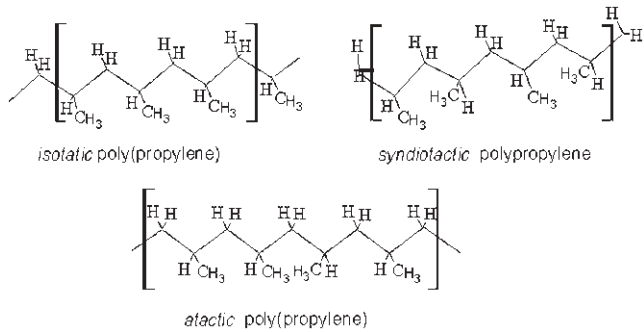

Figure 1.8 The tactic forms of polypropylene. Both the isotactic and syndiotactic forms have elements of symmetry and hence can crystallize, whereas the atactic form does not have a symmetry element and is amorphous.

1.3.2 Disordered or Amorphous Polymers

A polymer such as atactic polystyrene has a very bulky phenyl group pendant to the chain backbone and the groups are irregularly distributed in space. The phenyl groups are not favourably disposed to interact and crowding leads to a situation where the *trans* structure ceases to be the lowest energy state and energy profile simplifies to two conformations: an accessible *gauche* state and a distorted *trans* state. Using this approach, accurate simulations of the size of the isolated polymer molecule in dilute solution have been made.[23,24] In the solid state, polystyrene retains this disordered state and its morphology is that of an amorphous material. In general, if the polymer backbone contains a very bulky pendant group then it is highly probable that unless there are some very strong interactions the polymer will exhibit an amorphous structure in the solid state. The isotactic form of polystyrene allows the phenyl chains to interact in a favourable manner and crystalline forms are obtained from this polymer. Detailed studies of the kinetics of formation of the crystalline structure in this polymer system indicate that conformational dynamics are important in determining the observed behaviour.

1.4 Classification of Polymers

For flexible polymers, *i.e.* those that are able to undergo internal rotation about their backbones, the following classification can be made according to various constraints that we can place on the solidification process (Figure 1.9). There are two other classes of polymer worthy of mention: these are rigid rod like molecules where the shape of the polymer has a major effect on its ability to pack, and crosslinked polymers. In the latter system, the morphology of the polymers will be influenced by the size of the chain elements that exist between the network crosslinks. In a polymer system such as a silicone rubber, the

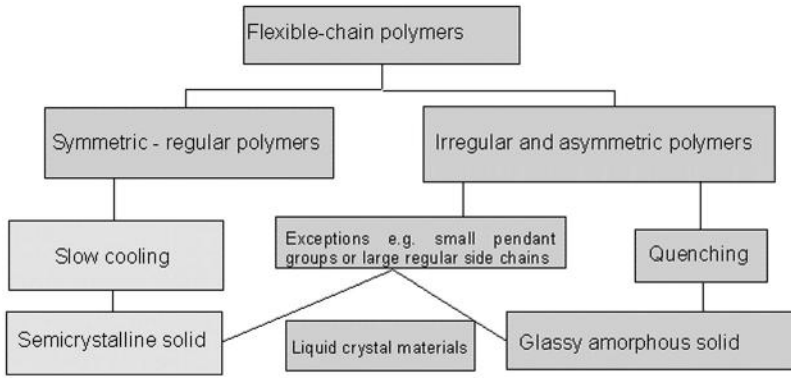

Figure 1.9 Classification of morphology by the chemical structural polymer type.

network dimensions may involve significant lengths of polymer chain and the resultant material is elastomeric. In contrast, an epoxy resin may be formed from relatively small chain elements and the high density of crosslinks results in the material being very rigid. The modulus of the material is dictated by two facts: the size of the polymer chain between the crosslinks and the conformational dynamics of that chain. If the barrier to internal rotation is high, as in the case of an aromatic-containing epoxy resin, then that material will be hard and glassy. If, as in the case of a typical silicone rubber created by the crosslinking of a polydimethylsiloxane (PDMS), the chain is flexible and an elastomeric material develops. Decreasing the molar mass of the PDMS results in a progressive increase in the chain–chain interactions and a subsequent increase in the modulus and hardness of the material until ultimately when the link is $–Si(Me)_2O–$ the material takes on glassy characteristics.

1.4.1 What Factors Determine Whether a Polymer will Form a Crystalline Solid or Not?

The regularity of the polymer backbone is the key factor; *isotactic* polypropylene crystallizes forming a rigid stable solid, whereas *atactic* polypropylene does not and forms a rubbery elastic solid. For flexible polymers, the structure of the solid is dictated by the symmetry of the polymer backbone. For the formation of a semi-crystalline solid it is necessary for there to be either an element of symmetry in the repeat unit chemical structure or strong interactions to aid the packing of the molecule and initiate the alignment that is required for the crystal growth process.

Atactic polymers do not crystallize, with two exceptions:

(i) When the X group in $(–CH_2CHX–)_n$ is very small, allowing regular packing of the chains regardless of whether the different pendant groups are randomly placed. Poly(vinyl alcohol) with its small hydroxyl X

group and strong polymer–polymer interactions is the kind of exception which demonstrates crystallization.

(ii) The X group forms a longer regular side chain. Side chain crystallization may occur provided that the pendant groups are of sufficient length, usually greater than about six repeat units.

Random copolymers, where the repeat units do not have a regular sequence structure, are incapable of crystallizing except when one of the constituents is at a significantly higher concentration than the other constituent. Linear low-density polyethylene with a crystallinity of about 50% contains 98.5 mol% of methylene units and about 1.5 mol% of CHX units, where X is $-CH_2CH_3$ or a longer homologue. Polymers that are potentially crystallizable may be quenched to a glassy amorphous state. Polymers with large side chains, or having an inflexible backbone chain are more readily quenched to an amorphous glassy state. The structure of the solid is therefore a combination of the intrinsic effects of the chemical structure and thermal factors involved in the creation of the solid.

Block copolymers, as we shall see later, are able to phase separate and it is possible for one of these phases to have semi-crystalline structure. Whether or not a crystalline phase is observed depends on the relative molar masses of the elements that form the polymer chain and their ability to pack into the required structure.

Polymers with rigid backbones, if they are sufficiently straight, will align like matchsticks and will either form 'liquid crystal' like structures or semi-crystalline mesomorphic phases.

Recommended Reading

P.J. Flory, *Statistical Mechanics of Chain Molecules*, Wiley Interscience, New York, 1969.
W.L. Mattice and U.W. Suter, *Conformational Theory of Large Molecules*, Wiley Interscience, New York, 1996.
M. Rubinstein and R.H. Colby, *Polymer Physics*, Oxford University Press, Oxford, 2003.

References

1. H. Staudinger, *From Organic Chemistry to Macromolecules*, Wiley-Interscience, New York, 1970.
2. H. Staudinger, *Chem. Ber.*, 1924, **57**, 1203.
3. H. Mark and G.S. Whitby (eds), *Collected Papers of Wallace Hume Carothers on High Polymeric Substances*, Wiley-Interscience, New York, 1940.

4. P.J. Flory, *Principles of Polymer Chemistry*, Cornell University Press, Ithaca, NY, 1953.
5. H. Morawitz, *Polymer: The Origins and Growth of a Science*, Wiley-Interscience, New York, 1985.
6. P.J.T. Morris, *Polymer Pioneers*, Centre for the History of Chemistry, Philadelphia, 1986.
7. C.E. Housecroft and E.C. Constable, *Chemistry*, Pearson Education, Essex, UK, 2nd edn, 2002, p. 242.
8. E. Wyn Jones and R.A. Pethrick, in *Topics in Stereochemistry*, ed. E.L. Eliel and N.L. Allinger, Wiley Interscience, New York, 1970, vol. 5, p. 205.
9. A.R. Ubbeholde, *The Molten State of Matter*, John Wiley, New York, 1978, p. 160.
10. K. Larsson, *J. Am. Oil Chem. Soc.*, 1966, **43**, 559.
11. L. Reinisch, *J. Chim. Phys. Physiochem. Biol.*, 1968, **65**, 1903.
12. R.A. Pethrick, M.A. Cochran, P.B. Jones and A.M. North, J. Chem. Soc., *Faraday Trans.*, 1972, **68**, 1719–1728.
13. H.J.M. Bowen and L.E. Sutton, *Tables of Interatomic Distances and Conformations in Molecules and Ions*, Chemical Society, London, 1958(Supplement 1965).
14. H.M.M. Shearer and V. Vand, *Acta Crystallogr.*, 1956, **9**, 379.
15. A. Abe, R.L. Jernigan and P.J. Flory, *J. Am. Chem. Soc.*, 1966, **88**, 631.
16. D.W. Scott, J.P. McCullough, K.D. Williamson and G. Waddington, *J. Am. Chem. Soc.*, 1951, **73**, 1707.
17. R.A. Pethrick, A.M. Awwad and A.M. North, *J. Chem. Soc., Faraday Trans. 2*, 1983, **79**, 731–743.
18. R.A. Pethrick, A.M. Awwad and A.M. North, *J. Chem. Soc., Faraday Trans.*, 1982, **78**, 1687–1698.
19. P.J. Flory, *Statistical Mechanics of Chain Molecules*, Wiley Interscience, New York, 1969.
20. W.L. Mattice and U.W. Suter, *Conformational Theory of Large Molecules*, Wiley Interscience, New York, 1996.
21. U.W. Gedde, *Polymer Physics*, Chapman & Hall, London, 1995.
22. M. Rubinstein and R.H. Colby, *Polymer Physics*, Oxford University Press, Oxford, 2003.
23. D.Y. Yoon, P.R. Sunderararajun and P.J. Flory, *Macromolecules*, 1975, **8**, 776.
24. R. Rapold and U.W. Suter, *Macromol. Theory Simul.*, 1994, **3**, 1.

CHAPTER 2

Crystal Growth in Small Molecular Systems

2.1 Introduction

Before considering the complexities of crystal growth in polymeric systems, we shall briefly look at the way in which small molecules form crystals. Slow cooling of the melt of an organic molecular system, such as benzophenone,[1,2] will lead to the growth of large single crystals, which can be several centimetres in size and have been a speciality of the research of Professor J. N. Sherwood at Strathclyde for many years (Figure 2.1).

In such a crystal, the molecules are ordered and adopt a minimum energy structure. Each of the faces will correspond to a particular orientation of the molecules within the crystal lattice. Because of the molecular orientations within the unit cell, the crystal faces may or may not have a different surface

Figure 2.1 A single crystal of benzophenone. The scale bar indicates 1 cm.

energy. In general, the single-crystal form of the material is a purer material than the *amorphous* disordered form.

Crystallization and crystal growth are very important parts of the manufacture of pharmaceutical chemicals and pigments. Paracetamol exhibits different crystal structures that have different solubilities.[3] The crystal growth process can be influenced by the presence of impurities that in general will be excluded from the growing crystal, but can in some cases be adsorbed on specific surfaces and influence growth. These molecules that modify the energy of specific faces are called *habit* modifiers. Impurities that have chemical structures that are similar to those of the bulk crystalline material can often be every effective *habit* modifiers. The exclusion of impurities from growing crystals forms an important method of purification for pharmaceutical and other fine chemicals. In certain cases impurities can be toxic and it is essential that they be removed from the pharmaceutical product. In some cases the impurities form the seeds from which the crystal growth is nucleated. To be able to predict the *morphology*—the bulk structure of the crystals—it is necessary to understand the factors that control the kinetics of the growth step and the influence of impurities on the growth process.

2.1.1 Crystal Types

The single crystals demonstrate elegant shapes as a result of the three-dimensional ordering of the molecular entities. The primary repeating pattern, the unit cell, replicates into the macro structures. Each entity sits at or near the intersection (lattice points) of an imaginary grid, the lattice (Figure 2.2). The smallest repeating unit is the asymmetric unit.

In Chapter 1 the unit cell for sodium chloride was presented (Figure 1.1). The periodic arrangement of any motif (e.g. group of atoms) of points located such that each has identical surroundings, produces an infinite arrangement that is called a *lattice*. The repeating period of the space lattice is called the *unit cell*. The *unit cell* contains a number (Z) of asymmetric units and it can be described by the dimensions a, b and c and the angles α, β and γ, with α being the angle between b and c, β between a and c and γ between a and b, *i.e.* $\alpha = \angle b.c$, $\beta = \angle a.c$ and $\gamma = \angle a.b$. These lengths and angles are the lattice constants or lattice parameters of the unit cell. The lattice parameters can for a crystalline

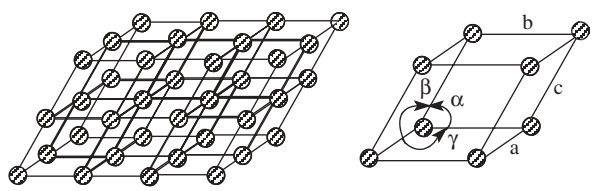

Figure 2.2 Crystal lattice (a) and the corresponding unit cell (b).

Table 2.1 The seven crystal systems and associated symmetry.[6,7]

Crystal system	*Cell parameters*	*Minimum symmetry*
Cubic	$a=b=c$; $\alpha=\beta=\gamma=90^\circ$	Four 3-fold rotation axes
Tetragonal	$a=b\neq c$; $\alpha=\beta=\gamma=90^\circ$	One 4-fold rotation or rotation–inversion axis
Orthorhombic	$a\neq b\neq c$; $\alpha=\beta=\gamma=90^\circ$	Three perpendicular 2-fold rotation or rotation–inversion axes
Trigonal	$a=b=c$; $\alpha=\beta=\gamma\neq 90^\circ$	One 3-fold rotation or rotation–inversion axis
Hexagonal	$a=b\neq c$; $\alpha=\beta=90^\circ$, $\gamma=120^\circ$	One 6-fold rotation or rotation–inversion axis
Monoclinic	$a\neq b\neq c$; $\alpha=\gamma=90^\circ\neq\beta$	One 2-fold rotation or rotation–inversion axis
Triclinic	$a\neq b\neq c$; $\alpha\neq\beta\neq\gamma\neq 90^\circ$	None

material be readily determined by X-ray or electron diffraction. Cells with only one unique motif are referred to as *primitive*. It is possible to generate a primitive cell from a given lattice, but in many cases end-, face- or body-centre representations are preferred because they may show greater symmetry than the primitive cells.

Bravais[4] postulated that there were fourteen different ways of arranging the lattice points in three-dimensional space. These are consistent with seven crystal systems that are listed in Table 2.1. The primitive lattice cell (P) has a lattice point only at the corner of the cell. Face centred (F) involves a lattice point at the centre of the opposite pairs of faces, while base centred (C) has a lattice point at the centres of the basal planes of the cell. Finally, body centred (I) involves a lattice point at the centre of the cell. The idealized Bravais structures are shown in Figure 2.3.

Crystals exhibit a high degree of symmetry. A number of different symmetry operations are possible on the lattice structures:

- Rotation around an n-fold axis, where the motifs are generated using cylindrical coordinates (r, ϕ), $(r, \phi+360^\circ/n)$, $(r, \phi+2\times360^\circ/n)$, *etc.*; n can take values 1, 2, 3, 4 or 6.
- Inversion centre located at (90, 0, 0) where the motifs are located at (x, y, z) and $(-x, -y, -z)$, x, y and z being Cartesian coordinates.
- Rotary-inversion axes, which involve a combination of rotation ($\alpha=360^\circ/n$) and inversion and are indicated by $\bar{n}$, which can take values $\bar{1}$, $\bar{2}$, $\bar{3}$, $\bar{4}$ and $\bar{6}$.
- Mirror planes.
- Screw axes, which involve a combination of translation along the screw axis and a rotation about the same. It is designated n_δ, where n is the rotation by an angle $\alpha=360^\circ/n$ and δ is an integer related to the translational component t, where $t=(\delta/n)c$, in which c is the length of the unit cell along the screw axis.
- Glide plane, which combines a translation in the plane and a reflection across a plane.

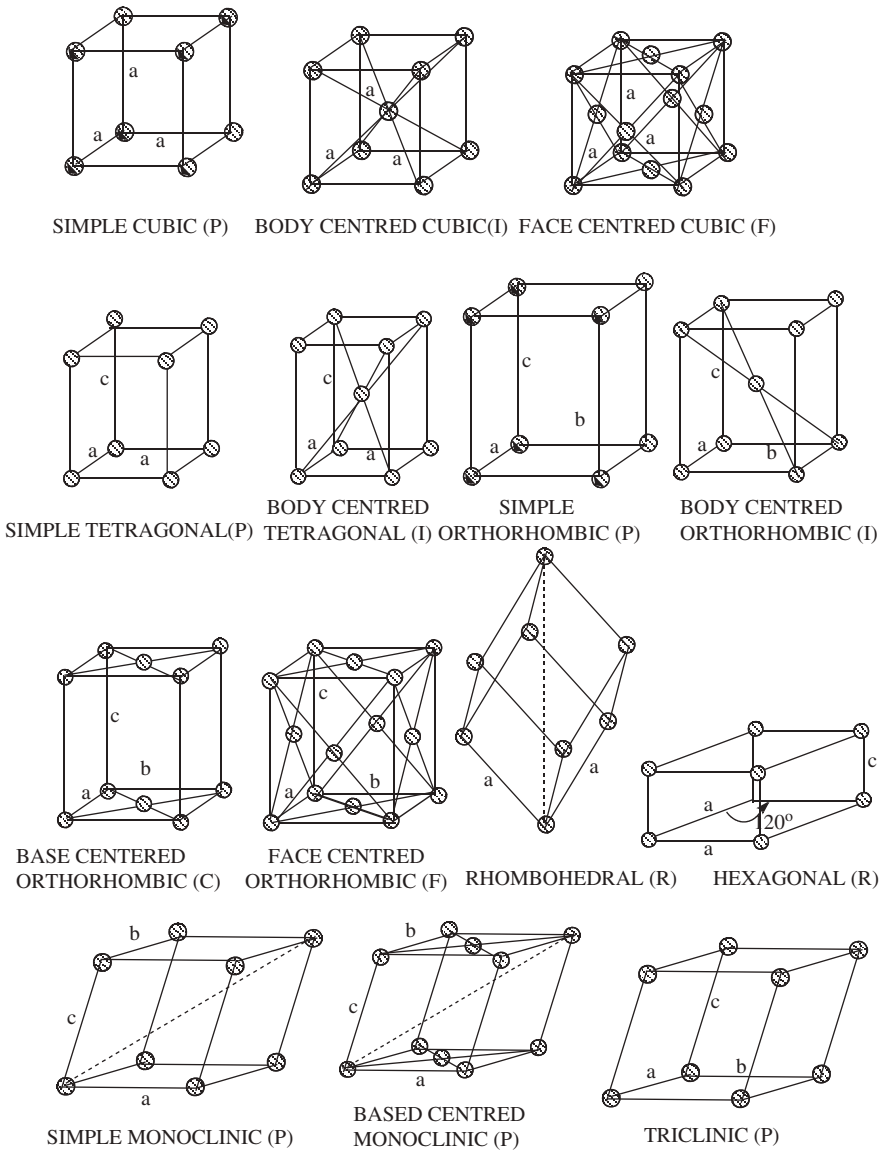

Figure 2.3 The fourteen Bravais lattices.[4]

The entire group of symmetry operators that completely describe the symmetry of the atomic arrangements within a crystal is called the *space group*. There are 250 space groups distributed among the 14 Bravais lattice groups. Another group of symmetry elements is the *point group*, which operates on the points that are usually groups or atoms. The allowed point group operators are rotation axes, axes of rotary inversion, inversion centres and mirror planes, and these altogether add up to 32 possible point groups.

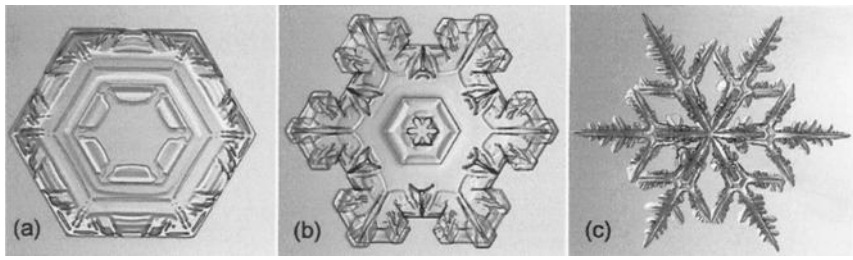

Figure 2.4 Examples of several different morphological types of snow crystals found in nature. Reproduced from reference 5.

The crystal is a *fractal* structure and the organization of the primitive unit cells can often be seen in the shape of the macroscopic crystal. A classic example of the *fractal* repetition of the unit cell is the crystalline structure of a snowflake.[5] The unit cells have the ability to build into a variety of complex shapes, yet each unit cell retains its perfect structure. The primary unit cell structure in the case of a snowflake is hexagonal and undergoes dendritic growth to produce an array of different macro crystals (Figure 2.4). The final shape of the snow crystal will depend on the conditions used in the growth process (temperature, humidity, *etc.*), which leads to a wide variety of observed *morphologies*.

In crystals, it is necessary to denote the plane directions and is done conventionally either by Miller's indices or by lattice planes. Directions are given as the lowest vector in referring to the coordinate system, $x(a)$, $y(b)$ and $z(c)$. A vector parallel to the chain axis is denoted [001]. The first plane intersects the origin of the coordinate system. The next plane intersects the three axes at $x = a/h$, $y = b/k$ and $z = c/l$. The task is to find an integral combination of h, k and l that is finally presented in parentheses (hkl). All planes containing the chain axis, *i.e.* those parallel to the chain, have the general formula (h, k, 0). The lattice index system indicates not only the orientation of the planes but also the shortest distance between planes. The set of planes denoted (010) is a subset of (020). The orientation of the two sets of planes is the same but the interplane distances (d_{hkl}) are different: $d_{010} = b$ and $d_{020} = b/2$.

Negative values of hkl are indicated by bars ($0\bar{1}0$). Several sets of planes appearing in highly symmetrical crystal structures may be denoted together with brackets of the type {hkl}, e.g. the planes in a cubic structure (100), (010), (001), ($0\bar{1}0$), ($\bar{1}00$), ($0\bar{1}0$) and ($00\bar{1}$) are denoted simply {001}.

Miller's index system is similar to the lattice plane index system but with the difference that the hkl values are the lowest possible integer values. The Miller's index notation for both the sets of planes with the lattice plane indices (010) and (020) is simply (010). Miller's indices thus provide information only about the orientation of the planes and disregard the interplanar distances involved.

The most densely packed diffraction planes along the chain axis for polyethylene are denoted (002) in the lattice plane notation. The distance between the lattice planes is thus $c/2 \approx 0.127$ nm. In the Miller's index notation they are

(001). Whereas in small molecule systems crystal planes are not necessarily obviously related to the molecular structure, in polymers packing of chains or helices will naturally generate layered structures and the relevance of the interplanar distance to the nature of the polymer–polymer interaction potential becomes more obvious.

The scattering data have to be analysed in terms of the reciprocal lattice. The reciprocal lattice is defined in terms of the translation vectors of the unit cell: $\bar{a}$, $\bar{b}$ and $\bar{c}$. A of set of vectors of the reciprocal cell, $\bar{a}^*$, $\bar{b}^*$ and $\bar{c}^*$, exists fulfilling the following conditions: $\bar{a}.\bar{a}^* = 1$, $\bar{a}.\bar{b}^* = 0$, $\bar{a}.\bar{c}^* = 0$, $\bar{b}.\bar{a}^* = 0$, $\bar{b}.\bar{b}^* = 1$, $\bar{b}.\bar{c}^* = 0$, $\bar{c}.\bar{a}^* = 0$, $\bar{c}.\bar{b}^* = 0$, $\bar{c}.\bar{c}^* = 1$. It can also be shown that: $\bar{a}^* = (\bar{b} \times \bar{c})/(\bar{a}.\bar{b} \times \bar{c})$; $\bar{b}^* = (\bar{c} \times \bar{a})/(\bar{a}.\bar{b} \times \bar{c})$; $\bar{c}^* = (\bar{a} \times \bar{b})/(\bar{a}.\bar{b} \times \bar{c})$.

The scalar product $\bar{a}.\bar{b} \times \bar{c}$ is equal to the volume of the unit cell, $\bar{a}^*$ is perpendicular to plane *bc*, $\bar{b}^*$ to plane *ac* and $\bar{c}^*$ to plane *ab*. In an orthorhombic cell, the reciprocal cell vectors are parallel to the original cell vectors: $|\bar{a}^*| = 1/|\bar{a}|$; $|\bar{b}^*| = 1/|\bar{b}|$; $|\bar{c}^*| = 1/|\bar{c}|$. The reciprocal of the reciprocal vectors (cell) is the original cell. Thus: $\bar{a} = (\bar{b}^* \times \bar{c}^*)/(\bar{a}^*.\bar{b}^* \times \bar{c}^*)$; $\bar{b} = (\bar{c}^* \times \bar{a}^*)/(\bar{a}^*.\bar{b}^* \times \bar{c}^*)$; $\bar{c} = (\bar{a}^* \times \bar{b}^*)/(\bar{a}^*.\bar{b}^* \times \bar{c}^*)$. In real space *hkl* is equal to a point ($\bar{r}^*$) in the reciprocal space: $\bar{r}^* = h\bar{a}^* + k\bar{b}^* + l\bar{c}^*$; thus $\bar{r}^*$ is perpendicular to (*hkl*) and the interplanar spacing (d_{hkl}) can be calculated from $d_{hkl} = 1/|\bar{r}^*|$. It is helpful to think of the reciprocal lattice representation of the crystal lattice in which the planes of the crystal are each represented by a lattice point of the reciprocal lattice. This point in reciprocal space is located in a direction from the origin that is perpendicular to the (*hkl*) planes in real space.

2.2 Crystallization

The processes of crystallization and crystal growth, like many other processes in chemistry, are controlled by thermodynamic and kinetic factors. Thermodynamics will dictate the preferred, lowest energy form, but the rate at which this is achieved will depend on the processes involved in the molecular attachment: kinetic factors. In the simplest model, the molecules are placed at the points of lowest energy on the ideal lattice structure. It is usually assumed that the entity that is being attached is a single molecule; however, it could also be a dimer or a cluster of molecules. In certain situations, for instance growth of benzoic acid from a non-polar solvent, the entity which may be involved is a dimer or higher order cluster:

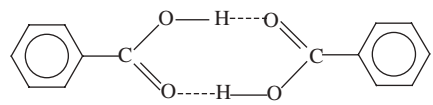

In the crystal lattice, the forces experienced by the molecule may be different from those that control the formation of the dimer in solution, and small but important conformational changes can occur that will influence the nature of the morphology generated. In general, the crystallizing entity will be solvated in

solution and its energy will reflect its interaction with the solvent molecules. Rearrangement of an entity that is initially attached to the surface may lead to a lower energy structure and this process is called Ostwald ripening.[8]

Crystal growth will usually be carried out from either the melt phase or from a saturated solution of the compound in a suitable solvent. The most perfect single crystals are grown from solution, and this process is the easiest to understand. Crystallization involves dissolving the pure compound in a solvent at high temperature and then lowering the temperature to a point at which *nucleation* occurs: stable clusters of molecules are formed. At the point of nucleation, the solubility of the material in the solvent has become critical and controls precipitation. The crystallization solution at this point has become *supersaturated*.[9,10] A solution that contains an excess of the solute at a given temperature is described as being supersaturated.

2.2.1 Supersaturation and Crystallization

Supersaturation is the essential driving force for all crystallization processes that occur from solution. Ostwald[8] first classified supersaturation in terms of 'labile', 'metastable' and 'supersaturated' depending on whether spontaneous nucleation did or did not occur (Figure 2.5). Crystallization can be promoted from solution either by cooling the solution, which leads to a decrease in solubility, or by evaporation. Crystal growth requires that nucleation should first occur and this can be achieved by one of a number of processes depending on the nature of the solution being examined.[9,10] Nucleation can be divided into two main processes: primary and secondary. The former is associated with growth from the melt in the absence (homogeneous) or presence (heterogeneous) of impurities. Secondary nucleation occurs if seed crystals are present in the mother liquid phase during nucleation.

At *supersaturation* the chemical potential of the solution and that of the solid that is formed on crystallization are equal:

$$\mu_{\text{solution}} = \mu_{\text{solid}} \tag{2.1}$$

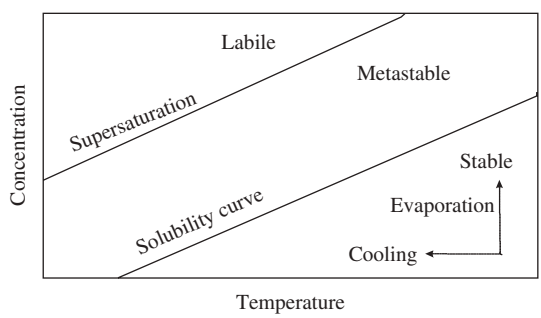

Figure 2.5 A typical solubility curve for a compound showing the three regions.[9,10]

where $\mu_{solution}$ is the chemical potential of the solute in solution and μ_{solid} is the chemical potential of the solute in the solid (crystalline) phase. If μ_{solid} is less than $\mu_{solution}$, *i.e.* $\Delta\mu = \mu_{solution} - \mu_{solid}$ is positive, the solution is said to be supersaturated and when $\Delta\mu$ is negative the solution is undersaturated. For crystal growth to occur, the solution has to be *supersaturated*. Because the chemical potentials of the solution and solid are often not easily determined, it is more common to express the supersaturation of a solution in terms of the concentration (c) of the solute in the solvent. The supersaturation is therefore the condition where the solute exists at a concentration in excess of its equilibrium solubility value and the free energy imbalance provides the driving force for crystal growth. The driving force from crystal growth is therefore determined by the magnitude of the concentration relative to the equilibrium solubility value. The relative supersaturation (σ) usually defined as a percentage value:

$$\sigma = \frac{c - c^*}{c^*} = S^{-1} \tag{2.2}$$

where c is the actual solute concentration, c^* is the equilibrium solute concentration and S is the supersaturation ratio. The value of c^* will depend on temperature and hence the value of σ will also be temperature dependent.

Depending on the initial concentration of the solute in the solvent, the point at which supersaturation is achieved will vary with temperature or through the process of solvent evaporation. The first process that is usually undertaken in order to successfully grow crystalline materials is the determination of the solubility curve in the growth solvent (Figure 2.5).

For a typical compound, the solubility diagram will exhibit three regions: the stable solution (low concentration–high temperature), metastable region and a labile region (high concentration–low temperature) where crystal growth occurs very rapidly. The stable region lies beneath the solubility curve and the solution is undersaturated and crystallization impossible. Cooling or evaporation increases the relative concentration to a point where the solution is now metastable and the solution is supersaturated and crystallization can be spontaneous. Within the metastable region, a solution can undergo controlled crystallization. Beyond this concentration region, the solution becomes increasingly unstable and a point is reached, supersaturation, at which instantaneous precipitation of the material is likely to occur.

2.3 Nature of Crystal Structures: Morphology and Habit

A rigorous terminology for the bulk shape of a crystal has been developed and leads to discussion of *morphology* and *habit*.[11] The morphology will depend upon the relative orientation and growth rates of the crystal faces. The growth velocity of a crystal face is measured by the outward rate of movement in a direction perpendicular to that face as shown in Figure 2.6. In most cases, for a

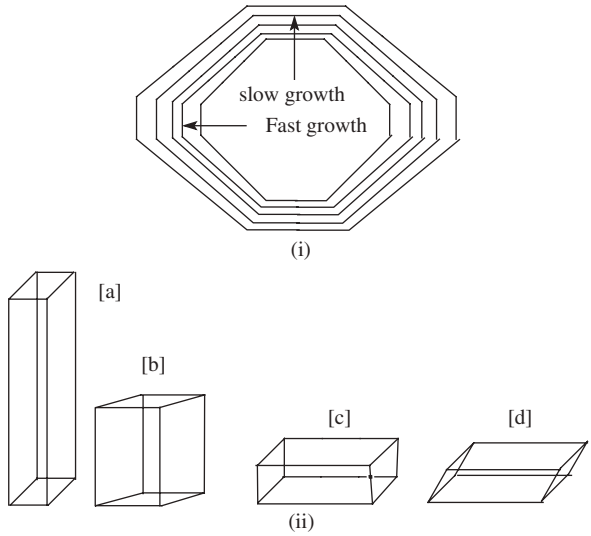

Figure 2.6 A schematic showing the effects of the different rates of growth on the crystal habits (a, b and c) and morphologies (c and d).

pure compound the velocity of growth will vary from face to face and reflects the nature of the orientation of the molecule within the unit cell of the crystal. If we examine the alignment of the molecule within the crystal, it is possible to identify which polar or functional groups will be orientated towards a particular face, with the result that the energy of each face is slightly different. The differences in energy of each face will in turn influence the growth rates for those faces. The shape of the crystal, or *habit*, is determined to a significant extent by the slowest growing faces.

The general shape that a crystal exhibits is defined as its *habit* (prismatic, needle-shaped or plate-like). The environment in which the crystal growth takes place will often influence the *habit* obtained. It is possible by changing the growth conditions to change the *habit* whilst retaining the same crystal morphology. In Figure 2.6 are presented various crystal *habits*: (a) prismatic, (b) needle-like and (c) plate-like. It is possible for a crystal to change its morphology but retain the same *habit*, this is illustrated in Figure 2.6c and 2.6d. Furthermore a crystal can change its *habit* and morphology, as shown in Figure 2.5a and 2.5d, where the *habit* has changed from being needle-like to plate-like and the crystal angles have changed.

2.3.1 Morphology Prediction

The morphology and *habit* exhibited by a crystal are controlled by a combination of the internal crystal structure of the unit cell and the external growth parameters. The morphology that is observed is in general a consequence of

two factors: the method of nucleation and the dominant factors influencing the growth of the crystal. The nucleation is controlled by the ability to form a stable cluster of molecules and crystal growth rate is determined by the ability of further molecules to become attached to the nucleus.[12] For simplicity we will consider initially the case of homogeneous growth from solution. As we will see later, the growth process can be subdivided into a series of sequential steps that reflect the way various factors influence the nucleation and growth processes.

2.4 Homogeneous Crystal Growth

The classical approach to crystal growth[13–17] considers the thermodynamic changes that occur on crystallization. The overall free energy difference, ΔG, between a small solid particle, the nucleus, and the solute in solution is the sum of the excess free energy between the surface of the particle and bulk of the particle, ΔG_s, and the excess free energy between a very large particle and solute in solution, ΔG_v:

$$\Delta G = \Delta G_s + \Delta G_v \tag{2.3}$$

Assuming that the clusters are spherical and have a radius r, then ΔG_s is a positive quantity proportional to r^2, while ΔG is a negative quantity proportional to r^3. Thus:

$$\Delta G = 4\pi r^2\gamma + \frac{4}{3}\pi r^3 \Delta G_\upsilon \tag{2.4}$$

where γ is the interfacial tension between the cluster and surrounding solution and ΔG_υ is the free energy change associated with the transformation per unit volume (Figure 2.7). Since ΔG_s and ΔG_v are of opposite sign and depend differently on the size of the growing crystal, the free energy of formation will pass through a maximum. Below the critical value, the nuclei that are formed are disrupted and dispersed before crystal growth can occur. Once this critical value has been reached the nuclei become stable and crystal growth can take place.

The maximum value, ΔG_{crit}, corresponds to the critical nucleus size, r_c. The value of the critical nucleus can be found by differentiating ΔG with respect to the radius of the nucleus in eqn (2.4) and setting $d\Delta G/dr=0$:

$$\frac{\partial \Delta G}{\partial r} = 8\pi r\gamma + 4\pi r^2 \Delta G_\upsilon = 0 \tag{2.5}$$

Thus

$$r_c = -\frac{2\gamma}{\Delta G_\upsilon} \tag{2.6}$$

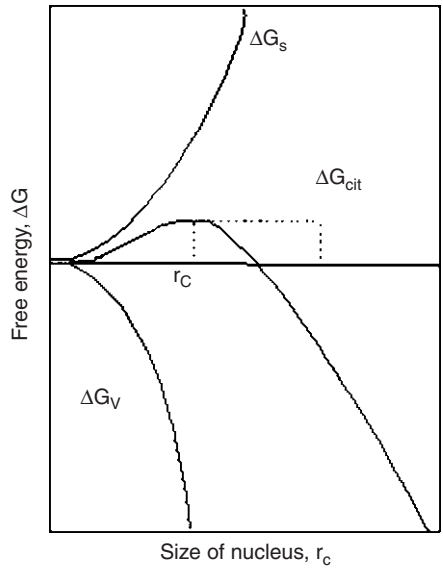

Figure 2.7 Free energy diagram for cluster formation.

Substituting eqn (2.6) into eqn (2.4) leads to

$$\Delta G_{\text{crit}} = \frac{16\pi\gamma^3}{3(\Delta G)^2} = \frac{4\pi\gamma r_c^2}{3} \tag{2.7}$$

This relation can be used with the free energy relationship:

$$\Delta G_{\upsilon} = \Delta H_{\text{v}} - T_{\text{c}}\Delta S_{\text{v}} \tag{2.8}$$

where ΔH_{v} and ΔS_{v} are the volume enthalpy and entropy of crystallization, respectively. At equilibrium, T_{c} is the equilibrium saturation temperature and $\Delta G_{\text{v}} = 0$. Equation (2.8) becomes

$$\Delta S_{\text{v}} = \frac{\Delta H_{\text{v}}}{T_{\text{c}}} = \frac{\Delta H_{\text{c}}}{V_{\text{m}} T_{\text{c}}} \tag{2.9}$$

where V_{m} is the molar volume. Given $\Delta T = (T_{\text{c}} - T)$ and using eqn (2.8) and (2.9) the following equation is obtained:

$$\Delta G_{\upsilon} = \frac{\Delta H_{\text{c}}}{V_{\text{m}}} - \frac{T\Delta H_{\text{c}}}{V_{\text{m}} T_{\text{c}}} = \left(\frac{\Delta H_{\text{c}}}{V_{\text{m}}}\right)\left(\frac{\Delta T}{T_{\text{c}}}\right) \tag{2.10}$$

For small supersaturations within the metastable zone (Figure 2.5), the degree of supersaturation can be related to the extent of under cooling (ΔT) through

the Gibbs–Thomson relationship:[15]

$$\ln(S) = \frac{\Delta H_c \Delta T}{k T_c^2} \tag{2.11}$$

where k is the Boltzmann constant. By eliminating ΔG_v and ΔH_c from eqn (2.6), (2.10) and (2.11) then

$$r^* = \frac{2\gamma V_m}{k T_c \ln(S)} \tag{2.12}$$

Equation (2.12) shows that the critical cluster size is inversely proportional to the degree of supersaturation. As the supersaturation increases so the critical size decreases and consequently the solutions become less and less stable. Crystal growth becomes a stable process because as the nuclei are formed the concentration of solute in solution is reduced and the system becomes thermodynamically stable. Substituting eqn (2.12) into eqn (2.7) gives

$$\Delta G_v = \frac{16\pi\gamma^3 V_m^2}{3k^2 T_c^2 [\ln(S)]^2} \tag{2.13}$$

The rate of nucleation, J, is the number of nuclei formed per unit time per unit volume. According to Becker and Döring,[14] J can be expressed by an Arrhenius type of relationship:

$$J = A \exp\left(-\frac{\Delta G^*}{kT}\right) \tag{2.14}$$

where A is the pre-exponential factor. Combining eqn (2.13) and (2.14), J can be expressed as

$$J = A \exp\left[-\frac{16\pi\gamma^3 V_m^2}{3k^3 T^3 [\ln(S)]^2}\right] \tag{2.15}$$

This equation indicates the complexity of the factors that influence the nucleation process: the temperature (T), degree of supersaturation (S), interfacial tension (γ) and molecular volume (V_m).

2.4.1 Empirical Description of Nucleation

An alternative method of modelling nucleation behaviour has been developed based on a kinetic approach.[17] In this model the mass nucleation rate, J_n, may be expressed by the following relationship:

$$J_n = K_n \Delta C_{max}^m \tag{2.16}$$

where K_n and m are the nucleation rate constant and nucleation reaction order, respectively. In eqn (2.16), ΔC_{max} is the maximum allowable supersaturation.

The nucleation rate can be expressed as

$$J_n = \left(\frac{\varepsilon}{1-(\varepsilon-1)}\right)\left[\left(\frac{\partial C^*}{\partial T}\right)\left(\frac{\partial T}{\partial t}\right)\right] \tag{2.17}$$

where T is the temperature, t is the time, dC^*/dT is the rate of concentration change with temperature and ε is the ratio of the molecular weights of solvated and unsolvated species. When solvation does not occur, the first term in eqn (2.17) is equal to unity. For a linear range of solubility, the metastable limit, ΔC_{max}, may be written as a function of the maximum allowable undercooling temperature ΔT_{max} before nucleation commences:

$$\Delta C_{max} = \left(\frac{\partial C^*}{\partial T}\right)\Delta T_{max} \tag{2.18}$$

At the metastable limit, a shower of nuclei produce sufficient surface area to prevent a significant further increase in supersaturation with respect to time. Due to cooling then:

$$\frac{\partial \Delta C}{\partial t} = 0 \text{ at } \Delta C_{max} \tag{2.19}$$

that is:

$$\frac{\partial C}{\partial t} = \frac{\partial C^*}{\partial t} = J_n \tag{2.20}$$

Hence at the metastable limit, the mass nucleation rate (or rate of change of concentration) is equal to the super saturation rate due to cooling. Equation (2.20) can be expressed in terms of the cooling rate, b (dT/dt):

$$J_n = b\left(\frac{\partial C^*}{\partial T}\right) \tag{2.21}$$

Equating eqn (2.16) and (2.21) for J_n gives

$$K_n \Delta C_{max}^m = b\left(\frac{\partial C^*}{\partial T}\right) \tag{2.22}$$

and substituting for the supersaturation in terms of eqn (2.21) gives

$$b\left(\frac{\partial C^*}{\partial T}\right) = K_n\left[\left(\frac{\partial C^*}{\partial T}\right)\Delta T_{max}\right]^m \tag{2.23}$$

Taking logarithms of eqn (2.23) gives

$$\log b = (m-1)\log\left(\frac{\partial C^*}{\partial T}\right) + \log K_n + m\log(\Delta T_{max}) \tag{2.24}$$

This equation indicates that the dependence of the logarithm of the maximum undercooling, ΔT_{max}, on the logarithm of the cooling rate, b, should be linear and the slope is equal to the nucleation reaction order, m.

The above theories do not consider in detail the growth process once the nucleation has occurred. Growth takes place via a number of steps and in principle is the same for both homogeneous and heterogeneous processes; however, in the latter we have to consider the possible influence of impurities on the relative rates of growth.

2.4.2 Stages of Crystal Growth

The incorporation of the growth units, single molecule or molecular cluster, onto a crystal face can be divided into several key stages. The processes can be visualized schematically as in Figure 2.8, and are designated as follows:

(i) *Bulk transport of the growth entity to the surface*. The solvated molecular entity or cluster of molecules first has to diffuse through a concentration gradient to the surface and may in the case of an ionic system have to pass through a boundary layer.
(ii) *Attachment of the growth entity to the surface*. The growth entity may in the simplest case be a single molecule, but may be a dimer, a cluster or a solvated species.
(iii) *Desorption*. Return of a growth entity or solvated species to the solution.
(iv) *Surface diffusion of the growth units to the step edge*. The absorbed entity, which may be a partially desolvated species, will move across the surface until it finds a suitable low-energy site. This might be a vacancy but is more probably a growing edge or dislocation. The edge or

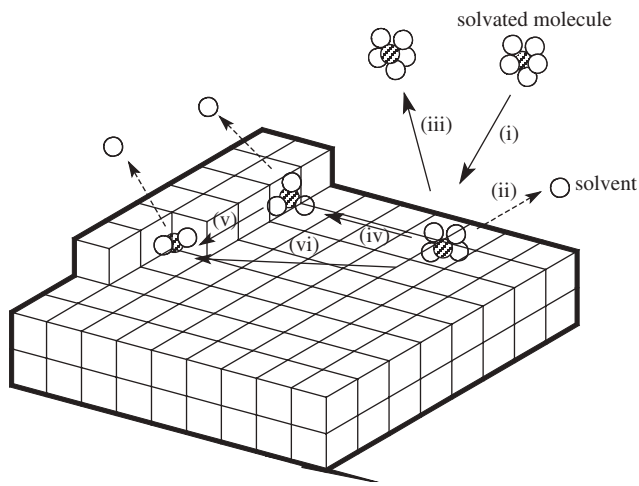

Figure 2.8 Schematic of the crystal growth process from solution. The crystallizing molecule is shown as the shaded circle and the solvent as the open circle.

dislocation will represent a lower energy state and hence the entity will become more strongly absorbed at these sites.

(v) *Migration of the growth unit along the step edge to a kink site*. The absorbed entity although in a low-energy site will still retain the ability to move as long as it is within a site of the same energy. Hence it is possible for an absorbed molecule to move along an edge to find a kink that will be of lower energy. As in the case of an entity absorbed on the surface, desorption from a step is always possible and hence migration to a kink is a mechanism whereby the probability of desorption is decreased.

(vi) *Volume diffusion to the step and direct integration of the growth units*. When the crystal is in equilibrium the processes above will be reversible, the rate of adsorption depending on the bulk concentration and the rate of desorption a function of temperature. As the bulk concentration is increased above the equilibrium value the rate of adsorption becomes greater than that of desorption and so the step will proceed to grow.

Whether or not this latter process occurs will depend on the relative energies of the binding at a particular site at which first attachment occurs to the energy of binding at an adjacent site.

At each stage in the process, loss of solvent molecules from the growth entity occurs and the free energy of the system is progressively lowered. The approach of the solvated entity to the surface will occur through a concentration gradient due to the depletion of material close to the growing surface. Once adsorbed (iv) the growth unit can diffuse across the surface to an energetically more favourable position such as a step or kink (v). The growth unit can alternatively be desorbed from the surface (iii) and return to the bulk solution. The growth unit is incorporated into the growing face once it attaches to a kink site (v). On a growing surface, kinks will be relatively abundant on the steps of a crystal. A 'flat face' step can therefore be seen as a continually changing surface that is never exactly flat and is a dynamic entity, as illustrated in Figure 2.9.

Whilst this analysis is appropriate for solution growth, similar situations will be developed in the melt, except the growing entity will often be a cluster of molecules. In both situations the formation of the step is a critical step in determining the final morphology of the material.

2.4.3 Heterogeneous Crystal Growth

In the case of crystallization from a melt, it has been observed that the rate of nucleation initially follows an exponential growth curve as the degree of undercooling is increased, reaching a maximum and subsequently decreasing.[15] This effect is attributed to the increase in viscosity as the melt is cooled inhibiting the nucleation process by suppressing the mobility of the entities from the nucleus moving, as illustrated from studies of crystallization of citric acid.[16]

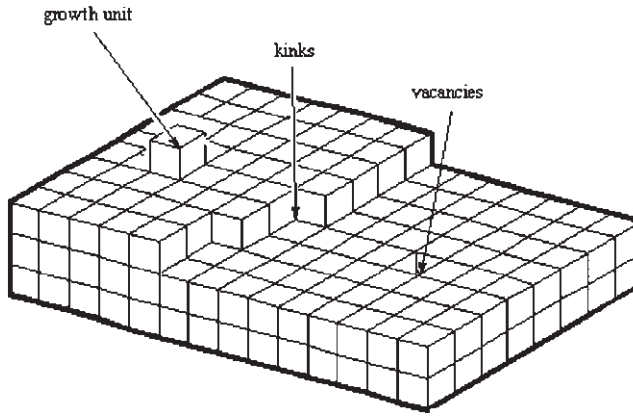

Figure 2.9 Schematic of a surface undergoing dynamic growth. In addition to kinks there will be isolated growth sites and also vacancies created by incomplete addition to steps.

2.4.4 Nucleation and Growth Rates

Whether it is homogeneous or heterogeneous growth, the nucleation rate J is difficult to measure, as the critical clusters formed correspond to a small number of molecules and hence are very small. In practice, the induction time (τ) is determined, which is the time between supersaturation and the first appearance of visible crystals. Assuming that the first appearance of the crystals is primarily controlled by the nucleation step, then τ is inversely proportional to the rate of nucleation:[18,19]

$$\tau = \frac{1}{\tau} \tag{2.25}$$

Combining eqn (2.15) and (2.25), the following is obtained:

$$\ln\left(\frac{1}{\tau}\right) = \ln(J) = \ln(A) - \left[-\frac{16\pi\gamma^3 V_m^2}{3k^3}\right]\left[\frac{1}{T^3[\ln(S)]^2}\right] \tag{2.26}$$

Using eqn (2.26), the interfacial energy can be evaluated from measurements of the induction time as a function of supersaturation. The radius of the critical nucleus can be derived from eqn (2.12).

Crystal growth is assumed to involve migration of the molecule or a cluster of molecules to a site on the surface that has a favourable energy of interaction. In order that a particular crystal face may grow, incorporation of growth units must occur in a sequential manner. The propagation of such successive growth layers will determine the overall rate of growth and hence the development of a particular morphology.

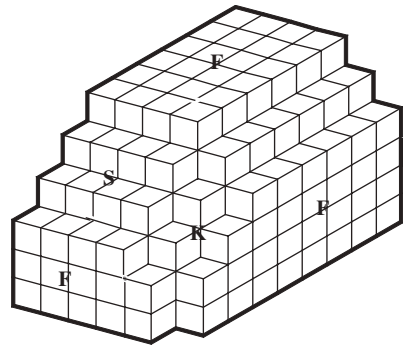

Figure 2.10 Designation of the flat surfaces (F), steps (S) and kinks (K).

2.4.5 Methods of Attachment to the Growth Surface

A growing crystal will not have perfectly flat surfaces and there are three types of face that can be identified: kinked (K), stepped (S) and flat (F) surfaces (Figure 2.10). This designation of the crystal surfaces is due to Kossel[20–22] and leads to the concept of surface roughening. A molecule adsorbed onto a kink site will be bounded on three sides whereas at stepped and flat surfaces the growth unit would only be bound by two sides and one side, respectively. Thus a face with a high density of kinks (K) would grow rapidly whilst flat faces (F) would grow the slowest. Any additional molecules adsorbed on the rough faces (the stepped and kinked faces) would never yield the even surfaces that are visible on most single crystals. It is therefore the flat faces that are observed to control the crystal growth.

2.4.6 Bravais–Friedel–Donnay–Harker Approach

Gibbs[12] attempted to predict the rate of crystal growth and indicated that the process required a minimization of the total free energy associated with the growing surfaces. It was subsequently shown that for a crystal at equilibrium, the faces generated are at a distance from the origin of the growth that is proportional to their individual surface energies. Developing this idea a simple three-dimensional plot of surface energy as a function of crystal orientation can be constructed. Bravais[4] and Friedel[23] used this concept to develop a simple method relating the internal structure to the morphology of a crystal.[24]

The Bravais law states that the morphologically most important forms would be those having the greatest interplanar spacings (d_{hkl}) and implies that the growth rates of the faces are inversely proportional to the interplanar crystal spacings. Donnay and Harker,[25] who developed rules relating the crystal symmetry to growth planes, refined the growth theory. These rules account for the effect of translational symmetry operators that cause the surface structure to be repeated more than once in the period d_{hkl}. For example, as we will explore later, the interplanar spacing of a face perpendicular to a 2_1

screw axis would be halved. The consequence of this consideration is that higher ordered planes can grow in preference to lower ordered ones.

The Bravais–Friedel–Donnay–Harker (BFDH) morphological simulations are based solely on lattice geometry and symmetry.[22,23] The BFDH simulations indirectly take into account the bond strengths present by considering slice thickness, but neglect mechanistic factors such as atom and bond types that also affect crystal growth. However, since these models are usually based on experimental observation they can help infer the dominant interactions that are controlling the crystal growth process.

The rate of crystal growth (R) predicted by the theory is expressed empirically as

$$R\alpha\frac{1}{d_{hkl}} \tag{2.27}$$

2.4.7 Periodic Bond Chains

Hartmann and others[24–27] have attempted to predict the morphology starting from consideration of the bonding within the crystal structure and the interactions between the crystallizing units. Their theory assumes that intermolecular forces govern the morphology of a crystal and identified the existence of uninterrupted chains of molecules 'strongly' bonded within crystal lattices, called periodic bond chains (PBCs). In PBC theory, the crystal growth mechanism is considered to involve the formation of consecutive bonds between crystallizing units during crystallization. A crystal network is made up of many different PBCs with differing energies that can be then classified into 'weak' and 'strong' PBCs. This concept is consistent with the idea that the energy of different faces will control the growth in the various observed directions. The theory leads to the idea of an 'attachment energy' (E_{att}) of a face, defined as the bond energy released per molecule when a new elementary growth layer, called a slice, of thickness d_{hkl} is attached to an existing crystal face. It is defined as

$$E_{\text{cr}}^{\text{ss}} = E_{\text{att}}^{\text{ss}} + E_{\text{sl}}^{\text{ss}} \tag{2.28}$$

where $E_{\text{cr}}^{\text{ss}}$ is the energy of crystallization and $E_{\text{sl}}^{\text{ss}}$ is the energy released on the formation of a growth slice of thickness d_{hkl}. The PBC theory assumes that rate of bond formation and hence the displacement velocity of a face will decrease with an increase in the attachment energy. Consequently the morphology that is developed is directly related to the attachment energy.[28,29] At low supersaturation the rate of crystal growth, R, is given by the following empirical relationship:

$$R\alpha E_{\text{att}}^{\text{ss}} \tag{2.29}$$

and provides a useful relationship for the prediction of the morphology of crystals grown below the roughening transition. To illustrate the way in which

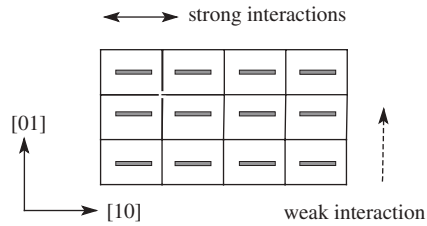

Figure 2.11 The way in which a simple two-dimensional morphology can be created using PBC theory.

growth occurs, we will consider the two-dimensional growth of a crystal which takes place predominantly in the horizontal direction (Figure 2.11).

In Figure 2.11, the strong interactions between the molecules lie along the horizontal direction and the weak interactions are perpendicular to the molecular axis. Therefore the growth will occur predominantly in the horizontal direction resulting in large (01) faces and small (10) faces. This simple situation will rarely occur and usually there will be interactions of varying strength between the molecules in various directions leading to more complex morphologies being observed.

In summary, for a crystal to grow in the direction of a strong bond the chain must be uninterrupted throughout the structure, and if a bond chain contains more than one type of bond it is the weakest bond present that determines the development of that orientation. Faces of a crystal can subsequently be classed into three types of faces according to periodic bond chains: F faces that have at least two PBC vectors parallel, S faces which are parallel to at least one PBC and K faces which have no PBC parallel.

2.4.8 Attachment Energy

For molecular materials, the strength of intermolecular interactions can be calculated by summing the interactions between a selected central molecule and each of the surrounding molecules within the crystal.[30] The simplest approach uses the atom–atom method in which the forces are assumed to be short range and involve the use of a van der Waals or similar potential modified to include dipolar terms. These calculations can be modified to include specific interactions such as hydrogen bonding, *etc*., and allow calculation of the crystal lattice energy that can be compared with the enthalpy of melting of the crystal. Scaling such calculations against measured heat of melting allows reasonable estimates to be made of the significant intermolecular bonds interacting and hence predictions of the morphology. The prediction of the morphology involves the calculation of the slice energy that is calculated by summing the interactions between a central molecule and all the molecules within a slice thickness d_{hkl}. Calculation of the attachment energy involves summing the interactions between a central molecule and all the molecules outside the slice. The centre of

the slice can be defined as the centre of gravity of a molecule or atom. The slice and attachment energies are then averaged over all these sites. As with PBC theory, the calculated attachment energies are directly related to the morphological importance of a crystal face. The rate of crystal growth, since it is related to the attachment energy, has the same proportionality as eqn (2.29).

2.4.9 Ising Model Surface Roughening

Growth at higher concentrations is assumed to involve addition of molecules to rough rather than to smooth surfaces. The Ising model is an attempt to describe the growth of a rough surface. A factor α has been introduced by Jackson[30] to describe the transition from smooth to rough growth. The factor α has the form

$$\alpha_{hkl} = \left(\frac{E_{\mathrm{sl}}}{E_{\mathrm{cr}}^{\mathrm{ss}}}\right)\left(\frac{\Delta H(T)^{\mathrm{diss}}}{RT}\right) \tag{2.30}$$

where $\Delta H(T)^{\mathrm{diss}}$ is the enthalpy of dissociation (or melting for melt growth). If we consider eqn (2.28) and (2.29) we can see that if the temperature increases, or if the in-plane surface intermolecular bonds, defined by $E_{\mathrm{sl}}^{\mathrm{ss}}$, decrease, α will decrease. At a critical value α_{c} that is approximately 2, an order–disorder phase transition takes place at the growth interface that becomes macroscopically rough.

- If α is larger than α_{c} the crystal face is in essence flat on an atomic scale and it has to grow by spiral growth or a two-dimensional nucleation mechanism, since an edge separating a solid and a fluid domain has an edge free energy larger than zero.
- If α is smaller than α_{c} one mixed solid–fluid phase occurs, the edge free energies are zero and the crystal interface solid surface is in essence rough and the crystal can grow without a layer mechanism. At this stage the overall crystallographic orientation (*hkl*) will also be lost.

In the Ising surface model the crystal fluid phase is partitioned at the interface between the solid and fluid, with the crystal interface considered as a gradient in solid and fluids cells, going from complete solid to a complete fluid phase. Using the concepts introduced by Onsager,[31] the dimensionless Ising temperature (θ_{ijk}) that corresponds to the order–disorder phase transition can be calculated:

$$\theta_{ijk} = \left(\frac{RT}{2\phi}\right)_{\mathrm{c}} \tag{2.31}$$

where ϕ is the strongest bond in the crystal lattice. By analogy with the α_{hkl} factors in eqn (2.30) we can define an experimental roughening factor

$$\theta = \frac{E_{\mathrm{cr}}^{\mathrm{ss}}}{\phi}\left(\frac{2RT}{\Delta H(T)^{\mathrm{diss}}}\right) \tag{2.32}$$

and thus for $\theta > \theta_c$ the crystal surface is rough and hence crystal growth will proceed.

The essential feature of any growth model is the recognition of the importance of steps in the growth process. The surface is not perfectly flat but will be covered with steps arising from various processes. Attachment involves the interaction of the absorbed growth entity with these steps.[32] The growth rate is therefore given by

$$R\alpha\frac{1}{\theta^{c}_{hkl}} \tag{2.33}$$

The principal difference between the above theories is the way in which attachment is treated to either a flat or rough surface. Aggregates of molecules on the surface form a nucleus for growth and will ultimately form a *step*; growth will also be possible at a dislocation.

2.5 Sources of Nucleation Sites on Surfaces, Steps and Dislocations

Any factors that can affect either the formation or movement of the growth entity will influence the type of morphology that is created, and therefore is a fundamental issue when considering crystal growth.

2.5.1 Two-Dimensional Nucleation

To gain some insight into the factors controlling step growth we will consider two-dimensional nucleation of growth. To create a layer on a flat surface, a stable cluster (Figure 2.8 and 2.9) has to form on which growth is initiated and step propagation will follow. In the two-dimensional nucleation mechanism, a growth unit will be adsorbed on the crystal surface and will require attachment of other units before stable growth can occur. During this stage the molecules attached to the surface will retain partially their solvation shells and will be able to move over the surface. As the growing units join up, the radius of the nucleus will increase and an increase in the free energy is observed (Figure 2.7) up to a maximum value. Further increase in the size of the nucleus leads to a decrease in the free energy. The size of the nucleus at which the free energy is a maximum is designated the critical radius, ρ_c, and is determined by eqn (2.6) and (2.7). If the nucleus radius is less than ρ_c it is unstable and dissolution is favoured; if the radius is greater than ρ_c it is stable and growth is favoured:

$$\rho_c = \frac{\omega\alpha}{kT\ln(1+\sigma)} \tag{2.34}$$

where ρ_c is the critical radius, ω is the unit volume of the growth unit, α is the free energy of the step edge, k is the Boltzmann constant, T is the absolute temperature and σ is the relative supersaturation.

Once a stable nucleus has been established, further growth can follow creating a new step on the flat surface and rapid growth will follow. For the process of step growth to be repeated another nucleus will have to be formed on this new surface and the nucleation step is the rate-determining process for the crystal growth. The theory predicts the probability of forming a nucleus is a very sensitive function of supersaturation and has been shown to be negligible at low supersaturations. Thus at low supersaturations growth would be expected to be zero if it were controlled solely by two-dimensional nucleation. However, experiment shows that contrary to prediction appreciable growth can occur at low degrees of supersaturation. The nucleation in these situations would appear to be easier than predicted by the theory and the ability to achieve growth at minimal supersaturation is attributed to the presence of imperfections in the crystals, called *growth defects*.

A further reason why growth becomes possible is the existence in solution of impurities that are able to nucleate crystal growth. Dust and other such material can nucleate crystallization and has to be carefully eliminated if perfect single crystals are to be grown.

2.5.2 Dislocations and Related Defects

2.5.2.1 Screw Dislocations

The occurrence of defects in the crystal lattice can act as nucleating sites for step growth and in particular dislocations with a screw component of the Burgers vector normal to that of the crystal face (Figure 2.12). The most important type of dislocation is a screw dislocation that causes a discontinuity in the crystal surface called a screw dislocation, which is a line defect in the crystal surface (Figure 2.12). The height displacement brought about by this slip creates a step

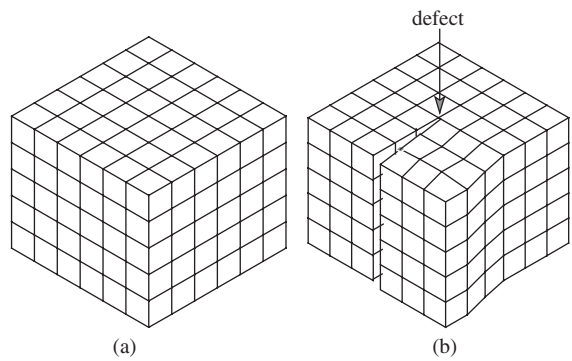

Figure 2.12 Dislocation in a crystal; the Burgers vector lying normal to the crystal.

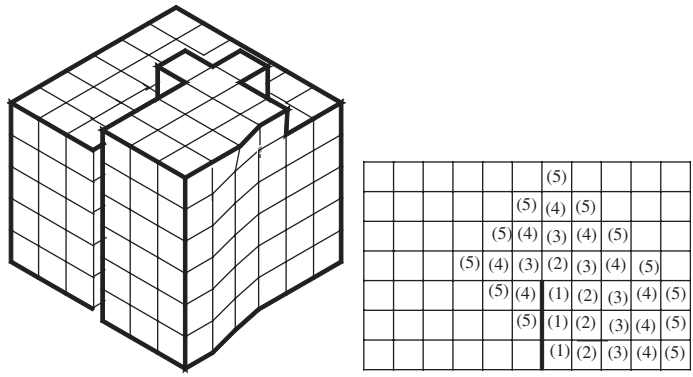

Figure 2.13 Schematic of growth at a dislocation that will lead to screw dislocation growth: (a) snapshot of the growth process; (b) sequence of adsorption of growth units around the defect leading to a screw climbing growth.

onto which the growth units can adsorb. Steps associated with the screw dislocation terminate at the dislocation. In order to propagate the step, growth will occur and wind around the dislocation (Figure 2.13). Away from the dislocation the steps advance relatively linearly and the number of the steps created per unit time by the dislocation determines the growth rate of the crystal. The critical radius of the two-dimensional nucleus restricts the curvature of the growth spiral: if the radius of the curve is less than ρ_c the advancing step will dissolve.

The initial attachment will occur at the dislocation, and the first layer, designated (1) in Figure 2.13, will follow closely the line of the defect. A second layer will easily be attached to the first line and will start to move the edge around the defect. Subsequent layers of attachment will move the edge around the defect and create the spiral growth indicated in Figure 2.13.

However, due to the upper surface being a spiral ramp, a completed growth layer is never obtained. Consequently the step will never disappear and growth can continue unperturbed. This mechanism eliminates the need for two-dimensional nucleation on which to construct new growth layers. A screw dislocation can be right handed, clockwise going from higher to lower level, or left handed, anticlockwise going from higher to lower level. Screw dislocations give rise to growth spirals and the distinction of 'handedness' becomes of importance when steps originating from distinct sources start to intersect. This mechanism has been observed in polymeric materials and will be illustrated later in the book.

2.5.2.2 Like Sign Dislocations

If two dislocation sources of the same sign (right or left handed) are very close together, less than half a step spacing, their spirals may join and form nonintersecting parallel spirals (Figure 2.14). These spirals effectively act as a

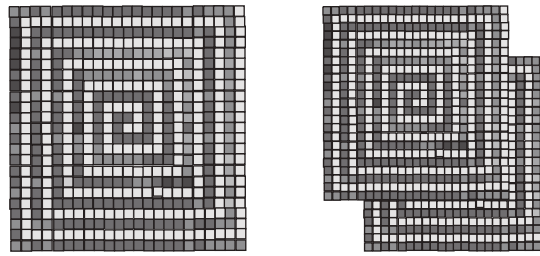

Figure 2.14 Two cooperating spirals (left), one depicted in white and the other in black; and two interlocking spirals (right).

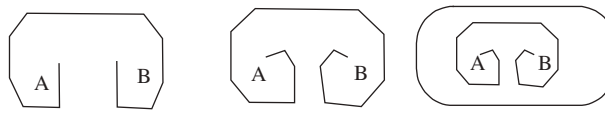

Figure 2.15 Progressive growth of two step dislocations of opposite sign (A and B).

single spiral but of double the height of a single spiral and are called co-operating spirals. The rate of step production per unit time would increase up to a factor of two depending on dislocation proximity and therefore increase the growth rate.

Alternatively if the same spirals were further apart, greater than half a step spacing, they would become a pair of interlocking spirals (Figure 2.14) and have the activity of one spiral. The less dominant spiral (the less developed spiral) would merely be contributory to the more dominant dislocation spiral. This case applies no matter how many screw dislocations are present; the most dominant spiral will still control the growth rate.

2.5.2.3 Opposing Sign Dislocations

If two dislocations of opposite sign emerge on a crystal face they will bridge to form a closed loop (Figure 2.15). This step will grow around both of the dislocations if the distance between the dislocations is greater than the critical diameter of the two-dimensional nucleus. The step grows and bows around the two dislocation points and eventually backs on to itself to form a completed loop.

Yet again as with other screw dislocations this ledge is a self-perpetuating step source and successive loops are formed without the need of nucleation. If the separation of the dislocations is less than the critical diameter, the step growth is prevented and the dislocation sources become inactive.

2.5.3 Screw Dislocation (BCF) Mechanism

Burton, Cabrera and Frank[33] have attempted to take into account the effect that occurs at low supersaturation and requires screw dislocations to provide a

permanent source of surface steps and hence binding sites for growth to proceed. The surface growth rate R is proportional to the supersaturation (σ) squared:

$$R \propto \sigma^2 \tag{2.35}$$

2.5.3.1 *Birth and Spread (B&S) Mechanism*

This mechanism occurs at moderate supersaturation and involves two-dimensional surface nucleation on a developing crystal.[34] The theory describes the growth of a layer from a nucleus that exists on a flat surface. The growth rate is roughly proportional to the exponential of the supersaturation:

$$R \propto \sigma^{5/6} \exp(\sigma) \tag{2.36}$$

2.5.4 Rough Interface Growth (RIG) Mechanism

At high supersaturation the rough interface growth mechanism occurs and the crystal grows without the presence of well-defined surface layers at the interface.[30] Due to the rough surface, the approaching entities are provided with numerous binding positions (Figure 2.10). This method of growth shows a linear dependence on supersaturation.

2.5.5 Relative Rates of Crystal Growth

Combining the predictions of the above theories it is possible to map the way in which the crystal growth rates vary with concentration.[35] The relative rates of the different processes are shown in Figure 2.16.

2.5.6 Computer Prediction of Morphology

Using the theories outlined above and simple force fields based on modified Lennard-Jones potentials of the type discussed in Chapter 1 it has been possible to calculate the morphologies that are predicted by theory.[32] The crystal morphology can be simulated using a classical Wulff plot[36] that computes the smallest polyhedron enclosed by the various crystal faces (*hkl*) using relative centre to face distances which are derived from the various models. Such projection of crystal shapes can be accomplished with the aid of the Gnomonic projection[37] that is made with the aid of available computer programs.[38] A computer program created by Roberts *et al.*[39–41] designated Habit has been used to examine a range of crystal morphologies. The predictions for the case of naphthalene are shown in Figure 2.17. In this case the Hartman–Perdok model (Figure 2.17c) and attachment model (Figure 2.17d) compare favourably with experiment. In other systems the other models have been shown to be successful.

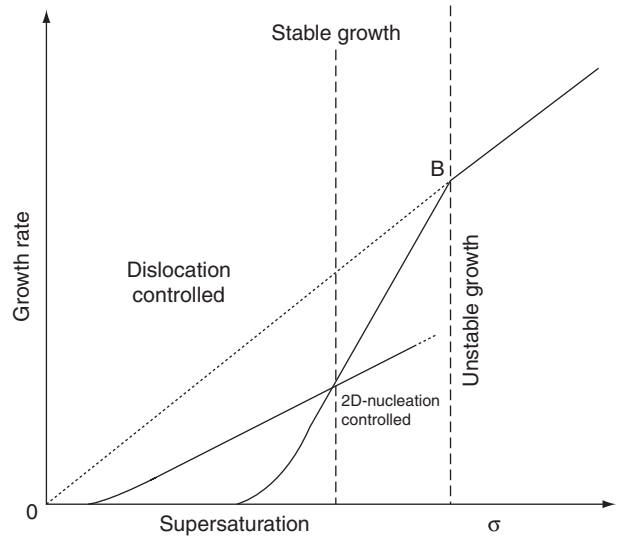

Figure 2.16 The relationship between growth rate and supersaturation showing the change from BCF to B&S to RIG mechanisms as the supersaturation increases.

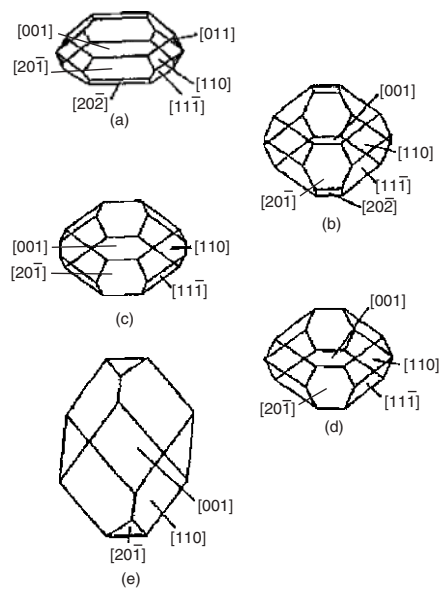

Figure 2.17 Results of the morphological simulation for naphthalene using various models in comparison with experiment: (a) experimentally observed morphology; (b) BFCH model; (c) Hartman–Perdok model; (d) attachment model; (e) Ising model.

2.6 Macrosteps

In the theories discussed above, it is assumed that the entity that is being absorbed is a single molecule or possibly a dimer. It is always possible that small clusters of molecules could be formed in the solution and diffuse to the surface. Thermodynamics would indicate that this is rather unlikely unless the entity has a radius that is greater than that required for nucleation. Therefore it is usually assumed that in conditions close to supersaturation such a mechanism is not very favourable. However, in a melt phase the possibility of larger entities being attached does now become possible and would lead to rough crystals.

The cluster that then attaches itself to the surface will undergo rearrangement, Oswald ripening, to achieve a lower energy structure. This structure, however, may not be the same as that which would be associated with the growth form dilute solution. It is assumed that the crystallizing entity will shed all the molecules of solvation in the region of the kink and it is the unsolvated species that is incorporated into the crystal. However, it is always possible that the strength of the solvation interactions can be sufficiently strong that the loss of the final solvent molecule is very slow. In such a situation the rate of step growth will be significantly slowed down. A further factor that can influence step growth is if it is possible to bunch the elementary steps. This is rather like cluster formation and leads to the formation of macrosteps and macro growth hillocks.

2.6.1 Impurities

Although the theory has been developed for homogeneous nucleation, in practice it is extremely difficult to produce materials that are completely free of impurities. In the presence of impurities the growth is heterogeneous. The addition of very small amounts of additives to the growth solution has been shown in many cases to have a marked effect on crystal growth. The impurities are often of two types: (i) impurities that occur in the compounds which reflect the method used in the synthesis of the compound and (ii) molecules that are added to the crystal growth solution to influence the morphology. The latter are called *habit* modifiers. They are usually molecules that have a structure that is similar to that of the molecule being crystallized but lack one of the functions. As such if they are incorporated into the lattice they will influence the balance of strong and weak forces (Figure 2.8). For instance, benzaldhyde will be a modifier for the growth of benzoic acid.

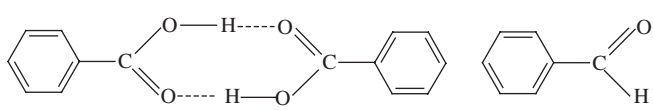

dimer - benzoic acid

benzaldehyde

The dimer of benzoic acid is a non-polar entity whereas the benzaldehyde monomer will have a significant dipole. It is therefore very important to purify organic materials to a very high level if one wishes to obtain the true crystal morphology. Generally, solutions may contain between 10^6 and 10^8 solid particles per cubic centimetre and these foreign particles can act to lower the interfacial energy necessary for cluster formation:[17]

$$\Delta G = 4\pi r^2(\gamma - \gamma_s) + \frac{4\pi r^3 \Delta G_v}{3} \tag{2.37}$$

where γ_s is the interfacial tension between the hetero-nuclei and any molecular nuclei present within the solution. Heterogeneous nucleation occurs at a lower supersaturation than homogeneous nucleation ($\gamma > \gamma_s$) and hence the induction time and degree of undercooling necessary for bulk crystallization is lowered. This equation assumes that the hetero-nuclei appear homogeneous throughout the solution. It is difficult to model mathematically heterogeneous nucleation.

Impurities will in general add to the step or kink and retard growth of the crystal. When impurities are adsorbed onto the terrace the progressing step becomes pinned behind it and to advance has to bow between the impurities. If the distance between the impurities is less then $2\rho_c$ the step curvature will be too great and the step will dissolve thus stopping further growth. Additives can affect all of the crystal faces in an equal manner but usually, due to the different structure of the steps in different crystallographic directions, an additive will affect all the faces to varying degrees. It is for this latter reason that sometimes a particular habit modifier is added to a crystallization system.

The low molecular weight hydrocarbon fragments in diesel fuel readily crystallize at temperatures around 0 °C and form platelets.[42,43] These platelets can in cold weather block filters in the fuel supply pipes and lead to the vehicle becoming immobilized. The addition of a *habit* modifier suppresses the crystal growth in one direction and, instead of plates being formed, needles are created. The needles have the ability to pass through the fuel filters and hence allow the vehicle to continue operation in cold conditions. This illustrates a positive use of impurities in the control of crystal growth.[44]

2.7 Analysis of the Data from Step Growth

Observation of the nature of the crystal faces (Figure 2.10) in terms of the relative areas of the flat (F) or rough (S or K) surfaces provides an indication of the growth mechanism (two-dimensional nucleation or screw dislocation). Measurements of the step height give an indication of the growth unit size, and the step spacing (the distance between advancing steps), y, allows an estimation of the critical radius (ρ_c). From the critical radius an approximation

of the step edge free energy can then be made:

$$y = 19\rho_c \tag{2.38}$$

and

$$\alpha = \frac{kT\sigma\rho_c}{\omega} \tag{2.39}$$

where ρ_c is the critical radius, ω is the volume of the growth unit, α is the step edge free energy, k is the Boltzmann constant, T is the temperature and σ is the supersaturation of the solution. Monitoring the proximity of two-dimensional nucleation (formation and dissolution) to step edges allows an approximation of the surface diffusion distance to be obtained. Moreover the measurement of step velocity gives an estimate of step kinetics. The effect of impurity addition can be classified from growth observation. Impurities can be adsorbed onto kinks, edges or terraces and affect none or all of the step directions. Examination of crystal growth with the addition of impurities can indicate the mechanism and extent of alteration that occurred. Recently the availability of atomic force microscopy (AFM) has allowed these previously inaccessible parameters to be determined experimentally[45–47] (Figure 2.18).

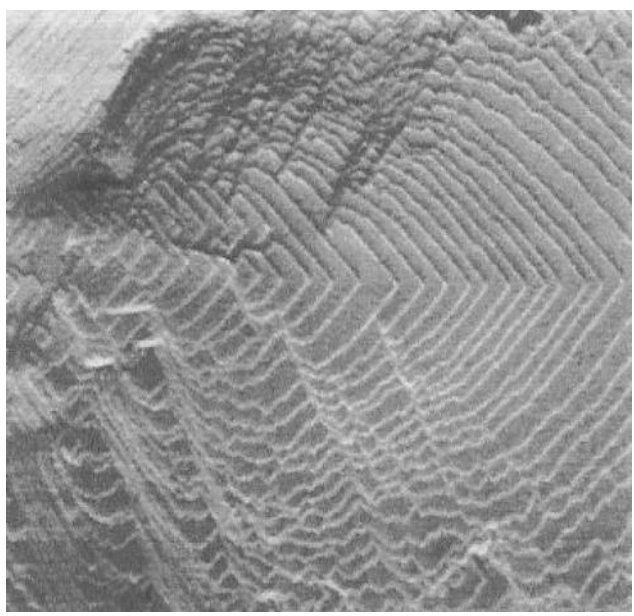

Figure 2.18 Atomic force microscopy images of an area 3.5 μm × 3.5 μm of poisoned growth of calcite.[46]

2.8 Refinements of the Theory

The principal challenge to the refinement of the theory is to describe accurately the processes associated with the migration of small clusters on the crystal surface and the consequent roughening processes that enhance crystal growth. As discussed above, one of the most difficult processes to model is the diffusion of the clusters across the surface and their entrapment at steps and defects. The physics of the diffusion of added atoms can be described by the Frank impurity mechanism using the BCF model of crystal growth.[48] The model is fundamentally two-dimensional and describes the quick formation of bunches of steps and their slower build-up in a lateral direction. In most regions, step bunches form quickly and equilibrium solutions to the equations can be developed. As pointed out in the discussion on modelling, in certain concentration ranges the Hartman–Perdok PBC theory has been found to be successful in its prediction of morphology.[49] Investigation of potassium dihydrogen phosphate (KDP), which is an ionic compound, presents particular challenges. The atomic structure at the outermost boundary is believed to control the growth mechanism and morphology of the crystal, while the presence or absence of cation–anion alternation at that boundary is supposed to determine the role of polarity in step kinetics. The observed pyramidal surface cell of KDP is considered to generate a strongly polarized growth front, but this may not always be the case. Surface electrostatics and the role of polarity on step kinetics cannot be inferred solely from the outermost ion array while ignoring the rest of the growth layer, including the step height. Cation–anion alternation at the surface termination is neither a necessary nor a sufficient condition for establishing surface polarity and, moreover, it does not necessarily imply alternation of positive and negative atomic charges on that plane. Consequently, and consistent with the symmetry point located in the middle of the experimentally determined d(101) layer cell of KDP, the observed pyramidal surface is unpolarized. The occurrence of the K^+-terminated, as opposed to the $H_2PO_4^-$-terminated, pyramidal surface of KDP grown out of an aqueous solution, as well as the role of ion impurities on the prismatic surface have been explained by this theory.

The use of computer modelling continues to advance and the integration of the Hartman–Perdok theory with the Ising theory for the roughening transition has been reported for the prediction of the crystal structures of venlafaxine, paracetamol and triacylglycerols.[50] An alternative approach to the description of the surface diffusion problem has been advanced also based on the BCF theory.[51] The flow of the solution over the surface influences the step bunching process. The flow within the solution boundary layer enhances step–step interactions and changes the resulting step pattern morphology on the growing surface.

The challenge to the theories is to be able to predict the various *polymorphs*—different morphologies that can arise when crystals are grown under different conditions.[51–53] The primary factors influencing polymorphism are solvent, temperature and impurities, *i.e.* habit modifiers. The recent use of computer predictions has allowed the development of a greater insight into the detailed factors that control the formation of particular morphologies.

2.9 Methods of Microstructural Examination

There are a number of methods now available for the examination of crystal morphology.[54] The shape can readily be determined by either optical or electron microscopy. Atomic force microscopy is now regularly used to study the surface of single crystals and considerable insight is being gained about the size of the steps and their relative location during the growth steps. The nature of the defect structure is somewhat more difficult to study. Imaging of defects that are features of the order of nanometres in dimension requires the use of X-ray diffraction methods. The usual method used is based on an approach put forward by Lang[55] and there are various experimental adaptations of these techniques:

(i) reflection topography[57–59]
(ii) transmission topography[55,60,61]
(iii) double crystal topography[56,62] and
(iv) white beam (synchrotron) topography.[63–68]

The Lang technique is shown in Figure 2.19. Incident X-rays enter a specimen crystal through a very narrow slit S_1 placed just before the crystal which is orientated to satisfy the Bragg diffraction condition. Since the X-rays are generated from scattering by an atom in the focal spot, they, even though collimated by the slit, have a divergency of the order of 100 seconds of arc. This degree of divergency is much larger than the intrinsic angular width of the diffraction peak for a perfect crystal that is of the order of 5 seconds of arc.[69] Therefore the incident wave must be regarded as a spherical wave that can be

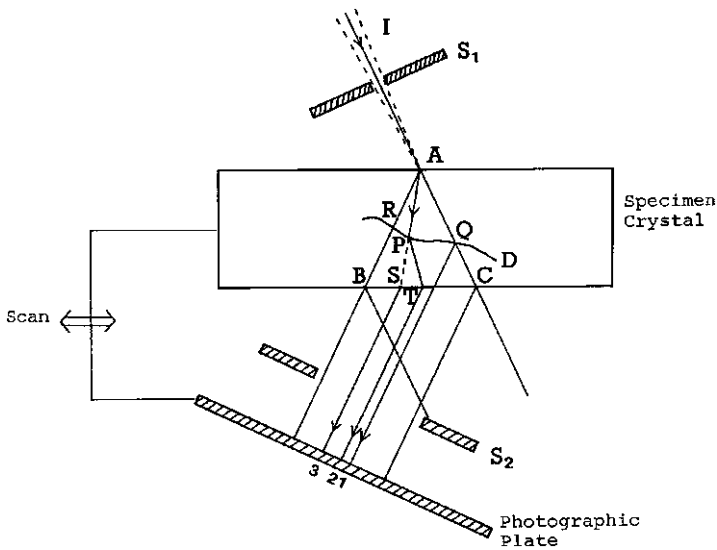

Figure 2.19 Schematic of the Laue X-ray diffraction experiment.

represented by a superposition of coherent waves. On entering the crystal, each reflecting plane aligned to satisfy the Bragg condition breaks every wave incident on it into two components, a transmitted and a diffracted wave. These waves interact with each other and set up two standing wave fields inside the triangular region ABC (Figure 2.19). This effect is know as anomalous transmission or the Borrmann effect[70,71] and the triangle ABC is called the Borrmann triangle. The Borrmann effect is one of the important consequences of the perfect periodicity of the lattice and provides a vivid demonstration of the dynamic theory of X-ray diffraction.

The two standing waves established in the Borrmann fan are Bloch waves of which the wave vectors differ. The difference in wave vectors leads to a difference in the propagation velocity and hence interference between the Bloch waves may occur. These interference effects, so-called Pendellösung effect, are observed in wedge-shaped crystals[72] and the resulting interference fringes are themselves a good indication of high crystal perfection.

The incident X-ray beam can be considered in two parts. A large part of the X-rays that do not satisfy the Bragg condition due to beam divergence pass straight through the crystal. This is called the direct beam. The remainder forms that part of the incident beam that satisfies the Bragg condition. Let us consider how these interact with defect D (Figure 2.19). Three types of defect image have been identified by Authier.[73] When the direct beam cuts the defect at Q, the misorientation due to lattice strain will cause a part of the beam to diffract. Thus the defect regions enhance the transmitted beam, increase its intensity and produce the so-called 'direct image' which appears black against a lighter background on the image plate. The limitation to this is the condition $\mu t > 10$, where μ is the X-ray absorption coefficient of the specimen and t is the thickness. Under this condition the direct beam suffers absorption within the sample and the direct image does not appear. This then defines the maximum usable thickness of the crystal. Within the Borrmann fan two types of image arise. On crossing the highly strained region at P the two waves decouple into their transmitted and diffracted components. When the waves re-enter the perfect part of the crystal they excite new wave fields. A part of the intensity is removed from the direction AP and the defect casts a shadow, producing the so-called 'dynamical image'. This is always less intense than the background and hence appears as a white image against a darker background. The newly created wave fields propagating along paths PT interfere with the original wave fields. The interference, which shows an oscillatory contrast, gives rise to the third type of image, the 'intermediary image', which has much poorer spatial resolution than the direct image.

In Figure 2.19, if the crystal and the photographic plate are stationary with respect to the incident beam, the recorded image is called a 'section topography' and represents a section through the crystal. If the crystal and plate are traversed together back and forth, the image is called a 'projection or transverse topography'. The projection topography integrates and records the full width of the crystal across the photographic plate. In projection topography dynamic and intermediary images become burred during the translation and are not well

contrasted, whereas direct images form relatively clear projections of defects. These are the predominately observed images.

White beam X-ray topography (Laue technique) is probably the simplest available X-ray imaging technique. Although the theory of defect contrast in white beam X-ray topography is not fully established, the principles are similar to those described for the X-ray Laue method.

Unlike characteristic line sources, the beam divergence of synchrotron radiation is very small, $\sim 10^{-5}$ rad. The direct image results from the contribution of those wavelengths that do not participate in the diffraction from the perfect crystal, rather than from the contribution of the divergent beam as in the case of a monochromatic experiment. Despite this, there is little qualitative difference between the images obtained using nearly zero divergence white beam sources and the corresponding images obtained from characteristic line sources.[74] In synchrotron topography the superposition of several harmonic reflections may be inevitable on each Laue spot. This obviously can cause some increased image width and line degradation compared with the source images.

The principal limitation of both techniques is the resolution achievable. For X-rays, dislocation image widths are ~ 1 μm. Thus the maximum resolvable defect content is $\sim 10^5$ dislocations per square centimetre. Since specimens of high quality are readily achievable this limitation presents few problems. An example of a large single crystal is shown in Figure 2.20 together with a Laue image of a slice taken from the crystal.[1] The 'g' in Figure 2.20a indicates the dominant growth direction for this crystal. Although the defects are clearly visible in the Laue images, these crystals represent almost perfect crystals from the point of view of organic crystal growth. The apparent doubling of the edge in the crystal view (Figure 2.20a) is a consequence of interference effects, the so-called Pendellösung effect, which is observed in wedge-shaped crystals. The observation of these rings is a good indication of a high degree of perfection in

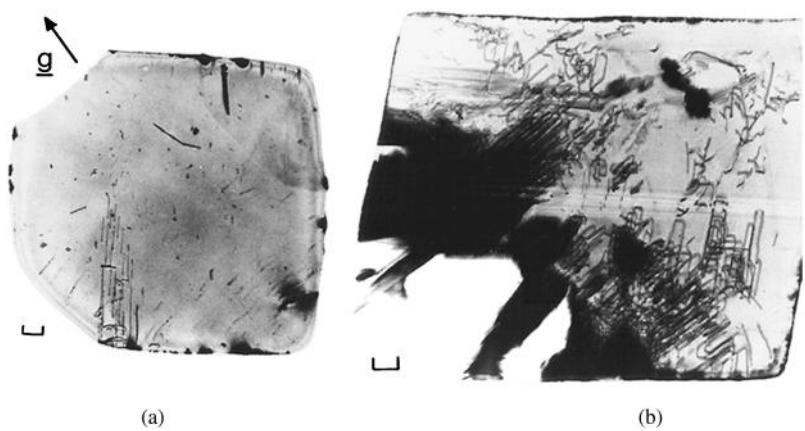

Figure 2.20 Single crystal of benzophenone viewed as a Lang diffraction image (scale bar = 1 mm): (a) a crystal grown from ethanol with low defect density; (b) a melt-grown crystal with high defect density.

the crystals. The crystal shown in Figure 2.20b illustrates the higher defect density that is associated with melt-grown crystals. It can clearly be seen that there are a number of slip and spiral dislocations. The higher rate of crystal growth in the latter system allows incorporation of a higher number of defects in the final crystal structure.

Recommended Reading

J.W. Mullin, *Crystallization*, Butterworth-Heinemann, London, 3rd edn, 1993.
O. Sohnel and J. Garside, in *Precipitation: Basic Principles and Industrial Applications*, Butterworth-Heinemann, London, 1991.

References

1. C.S. Yoon, J.N. Sherwood and R.A. Pethrick, *Philos. Mag. A*, 1992, **65**(5), 1033–1047.
2. H.X. Cang, W.D. Huang and Y.H. Zhou, *Prog. Natural Sci.*, 1996, **6**(2), 235–242.
3. H.M. Cuppen, G.M. Day, P. Verwer and H. Meekes, *Cryst. Growth Design*, 2004, **4**, 1341–1349.
4. A. Bravais, *Etudes Crystallographiques*, Gauthie-Villars, Paris, 1866.
5. K.G. Libbrecht, *Rep. Prog. Phys.*, 2005, **68**(4), 855–895.
6. A.S. Myerson and R. Ginde, *Handbook on Industrial Crystallization*, ed. A.S. Myerson, Butterworth-Heinemann, London, 1993.
7. A.G. Walton, in *Nucleation*, ed. A.C. Zettlemoyer, Marcel Dekker, New York, 1969, pp. 225–307.
8. W. Ostwald, *Z. Phys. Chem.*, 1897, **22**, 289–330.
9. J. Garside and M.A. Larson, *J. Cryst. Growth*, 1986, **76**, 88–92.
10. L.N. Balykov, M. Kitamura and I.L. Maksimov, *Phys. Rev. B*, 2004, **69**(12), 125411.
11. J. Prywer, *Cryst. Growth Design.*, 2002, **2**(4), 281–286.
12. W.J. Gibbs, *Collected Works*, Longman Green, New York, 1928.
13. M. Volmer, *Kinetic der Phasenbildung*, Steinkoff, Dresden, 1939.
14. K. Becker and W.E. Döring, *Ann. Phys.*, 1935, **5**(24), 719–752.
15. G. Tamman, in *States of Aggregation* (translated by R.F. Mehl), Van Nostrand, New York, 1925.
16. J.W. Mullin and C.L. Leci, *J. Cryst. Growth*, 1969, **5**, 75–76.
17. J.W. Mullin, *Crystallization*, Butterworth-Heinemann, London, 3rd edn, 1993.
18. G.H. Nancollas and N.Q. Purdie, *Rev. Chem. Soc.*, 1964, **18**, 1–20.
19. O. Sohnel and J. Garside, *Precipitation: Basic Principles and Industrial Applications*, Butterworth-Heinemann, London, 1991.
20. V.V. Voronkov, *Sov. Phys. Crystallogr.*, 1968, **13**, 13.

21. D.E. Temkin, *Sov. Phys. Crystallogr.*, 1969, **14**, 179.
22. H.M. Cuppen, H. Meekes, E. Van Veenendaal, W.J.P. van Enckevort, P. Bennema, M.F. Reedijk, J. Arsic and E. Vlieg, *Surf. Sci.*, 2002 **506**, 183.
23. G. Freidel, *Lecon de Cristalographic*, Herman, Paris, 1911.
24. A.A. Chernov, *Acta Crystallogr.*, 1998, **54**(6), 859–872.
25. J.D.H. Donnay and D. Harker, *Ann Mineral.*, 1937, **22**, 446–467.
26. P. Hartmann and W.G. Perdok, *Acta Crystallogr.*, 1955, **8**, 49–52.
27. C.S. Strom, *J. Cryst. Growth*, 2001, **222**, 298–310.
28. P. Bennema, *J. Cryst. Growth*, 1996, **166**, 17–28.
29. F.F.A. Hollander, M. Plomp, J. van de Streek and W.J.P. van Enckevort, *Surf. Sci.*, 2001, **471**(1–3), 101–113.
30. K.A. Jackson, *Liquid Metals and Solidification*, American Society of Metals, Cleveland, OH, 1958.
31. L. Onsager, *Phys Rev.*, 1944, **65**, 1117.
32. K.J. Roberts, R. Docherty, P. Benema and L.A.M.J. Jetten, *J. Phys. D: Appl. Phys.*, 1993, **26**, B7–B21.
33. W.K. Burton, N. Cabrera and F.C. Frank, *Phil. Trans. R. Soc. London, Ser. A*, 1951, **243**, 299–358.
34. G.H. Gilmer and K.A. Jackson, in *Crystal Growth and Materials*, ed. E. Kaldis and H.J. Scheel, North Holland, Amsterdam, 1974, pp. 80–114.
35. R. Dochert, Modelling the morphology of molecular crystals, PhD thesis, University of Strathclyde, 1989.
36. G. Wulff, *Z. Krist. Min.*, 1901, **34**, 499.
37. F.C. Phillips, *An Introduction to Crystallography*, Longmans Green, London, 1963.
38. E. Dowty, *Am. Mineral.*, 1980, **65**, 465.
39. R. Docherty, G. Clydesdale, K.J. Roberts and P. Bennema, *J. Phys. D: Appl. Phys.*, 1991, **24**, 89.
40. R. Docherty and K.J. Roberts, *J. Cryst. Growth*, 1988, **88**, 159.
41. R. Docherty, K.J. Roberts and E. Dowty, *Comput. Phys. Commun.*, 1988, **51**, 423.
42. A.R. Gerson, K.J. Roberts and J.N. Sherwood, *J. Cryst. Growth*, 1993, **128**(1–4), 1176–1181.
43. A.R. Gerson, K.J. Roberts and J.N. Sherwood, *Acta Crystallogr. B*, 1991, **47**, 280–284.
44. A.R. Gerson, K.J. Roberts and J.N. Sherwood, *Powder Technol.*, 1991, **65**(1–3), 243–249.
45. F.F.A. Hollander, M. Plomp and J.P. Van De Streek, *Surf. Sci.*, 2001, **471**, 101–113.
46. R.E. Hillner, S. Manne, P.K. Hansma and A.S.J. Gratz, *Faraday Discuss.*, 1993, **95**, 191–197.
47. S. Hodgson, PhD thesis, University of Strathclyde, 2003.
48. C.R. Connell, *Physica D: Nonlinear Phenom.*, 2004, **189**(3–4), 287–316.
49. C.S. Strom, *J. Cryst. Growth*, 2001, **222**(1–2), 298–310.

50. P. Bennema, H. Meekes, S.X.M. Boerrigter, H.M. Cuppen, M.A. Deij, J. van Eupent, P. Verwer and E. Vlieg, *Cryst. Growth Design*, 2004, **4**(5), 905–913.
51. A.A. Chernov, *J. Cryst. Growth*, 2004, **264**(4), 499–518.
52. K. Sato, *J. Phys D*, 1993, **26**, B77–B84.
53. J. Bernstein, *J. Phys D*, 1993, **26**, B66–B76.
54. R.A. Pethrick, in *Techniques for Polymer Organisation and Morphology Characterisation*, ed. R.A. Pethrick and C. Viney, Wiley, London, 2003.
55. A.R. Lang, *J. Appl. Phys.*, 1958, **29**, 597.
56. U. Bonse and E. Kappler, *Z. Naturforsch.*, 1958, **13a**, 348.
57. W.F. Berg, *Naturwissenschaften*, 1931, **19**, 391.
58. C.S. Barrett, *Trans. AIME*, 1945, **161**, 15.
59. H. Barth and R. Hosemann, *Z. Naturforsch.*, 1958, **13a**, 792.
60. A.R. Lang, *Acta Crystallogr.*, 1957, **10**, 839.
61. A.R. Lang, *Acta Crystallogr.*, 1959, **12**, 249.
62. W.L. Bond and J. Andrus, *Am. Mineral.*, 1952, **37**, 622.
63. U. Bonse, in *Direct Observation of Imperfections in Crystals*, ed. J.B. Newkirk and J.K. Wernick, Wiley, New York, 1962, p. 431.
64. A. Gunier and J. Tennevin, *Acta Crystallogr.*, 1949, **2**, 133.
65. L.G. Schultz, *Trans. AIME*, 1954, **200**, 1082.
66. T. Tumoi, K. Naukkarinen and P. Rabe, *Phys. Status Solidi A*, 1974, **25**, 93.
67. J. Miltat, in *Characterisation of Crystal Growth Defects by X-ray Methods*, ed. B.K. Tanner and D.K. Bowen, Plenum Press, New York, 1980, pp. 401–420.
68. M. Hart, in *States of Aggregation* (translated by R.F. Mehl), Van Nostrand, New York, 1925, pp. 421–432.
69. M. Sauvage, in *States of Aggregation* (translated by R.F. Mehl), Van Nostrand, New York, 1925, pp. 433–455.
70. G. Borrmann, *Z. Phys.*, 1941, **42**, 157.
71. G. Borrmann, *Z. Phys.*, 1950, **127**, 297.
72. D.J. Fathers and B.K. Tanner, *Philos. Mag.*, 1973, **28**, 749.
73. A. Authier, *Adv. X-ray Anal.*, 1967, **10**, 9.
74. B.K. Tanner, O. Midgley and M. Safa, *J. Appl. Crystallogr.*, 1977, **10**, 281.